The Ghost Fluid Method for deflagration and detonation discontinuities

Ronald P. Fedkiw *
Tariq Aslam †
Shaojie Xu ‡

October 26, 1998

Abstract

The level set method for compressible flows [17] is simple to implement, especially in the presence of topological changes. However, this method was shown to suffer from large spurious oscillations in [13]. In [5], a new Ghost Fluid Method (GFM) was shown to remove these spurious oscillations by minimizing the numerical smearing in the entropy field with the help of an Isobaric Fix [6] technique. This GFM was designed for traditional contact discontinuities where the interface moves with the fluid velocity only. In this paper, we extend the GFM to multi-material interfaces where the interface velocity includes a regression rate due to the presence of chemical reactions converting one material into another. As a specific example, we will consider interface models for deflagration and detonations discontinuities similar to the work in [22, 16, 23, 24]. The resulting numerical method is robust and easy to implement along the lines of [21].

*Research supported in part by ONR N00014-97-1-0027 and ONR N00014-97-1-0968

†Los Alamos National Laboratory - performed under the auspices of the U.S. Department of Energy

‡University of Illinois at Urbana-Champaign - Research funded by the U.S. Department of Energy through the University of California under Subcontract number B341494

1 Introduction

In [17], the authors applied the level set method to multiphase compressible flow. The level set function was used as an indicator function and each grid point was designated as one fluid or the other in order to choose the appropriate equation of state. Then the numerical fluxes were formed and differenced in the usual manner, see e.g. [21]. In [13], it was shown that this technique produced large spurious oscillations in the pressure and velocity fields. This problem was rectified in [10], [4], and [3] with schemes that involved *explicit* treatment of the appropriate boundary conditions at the interface. As a consequence, these schemes are intricate in one dimension and can only be extended to multiple dimensions with ill-advised dimensional splitting in time. In addition, multilevel time integrators, such as Runge Kutta methods, are difficult to implement for these schemes.

The Ghost Fluid Method (GFM) [5] avoids the oscillations at multimaterial interfaces without *explicitly* applying the interface boundary conditions. Instead, the GFM creates an artificial fluid which *implicitly* captures the boundary conditions at the interface. In the flavor of the level set method which *implicitly* captures the location of the interface, the GFM *implicitly* captures the boundary conditions at the interface. Since the boundary conditions are *implicitly* captured by the construction of a ghost fluid, the overall scheme becomes easy to implement in multidimensions without time splitting. In addition, Runge Kutta methods are trivial to apply.

In [5], the GFM was implemented for contact discontinuities where the interface moves at the fluid velocity only. In this case, the pressure and normal velocity of the ghost fluid are copied over from the real fluid in a node by node fashion while the entropy and tangential velocities are defined with the use of a simple partial differential equation for one-sided constant extrapolation in the normal direction. See [5] for details.

In this paper, we will extend the GFM to multimaterial interfaces where the interface velocity includes a regression rate due to the presence of chemical reactions converting one material into another. As a specific example, we will consider interface models for deflagration and detonation discontinuities similar to the work in [22], [16], [23], and [24] where the authors extended the level set method from [25] to interfaces that represent burning front discontinuities. In [25], the authors keep a sharp interface location using the

level set function, while smearing out the surrounding flow variables, e.g. density. This numerical treatment is not acceptable for deflagration wave discontinuities since their propagation speed is evaluated as a function of the exact unburnt gas conditions which are lost when the state variables are smeared out. In [22], [16], [23], and [24] the authors developed a new "in-cell reconstruction" technique that gives a sharp representation of the states on each side of the interface as needed for deflagration discontinuities. Those authors used the level set method to *implicitly* capture the interface location, while using the "in-cell reconstruction" technique to *explicitly* enforce the boundary conditions at the interface. The resulting algorithm is more efficient than standard interface tracking techniques, since the interface location is captured and not tracked. While the algorithm described in [22], [16], [23], and [24] utilizes dimensional splitting in time, this is not a necessary condition for the "in-cell reconstruction" technique [12]. However, the boundary conditions are still *explicitly* applied. In contrast, the GFM will *implicitly* capture the boundary conditions at the interface by the construction of a ghost fluid. The resulting numerical method is easy to implement in multidimensions (without time splitting) and extends trivially to Runge Kutta methods.

2 Equations

2.1 Euler Equations

The basic equations for compressible flow are the Euler equations,

$$\vec{U}_t + \vec{F}(\vec{U})_x + \vec{G}(\vec{U})_y + \vec{H}(\vec{U})_z = 0 \tag{1}$$

which can be written in detail as

$$\begin{pmatrix} \rho \\ \rho u \\ \rho v \\ \rho w \\ E \end{pmatrix}_t + \begin{pmatrix} \rho u \\ \rho u^2 + p \\ \rho uv \\ \rho uw \\ (E+p)u \end{pmatrix}_x + \begin{pmatrix} \rho v \\ \rho uv \\ \rho v^2 + p \\ \rho vw \\ (E+p)v \end{pmatrix}_y + \begin{pmatrix} \rho w \\ \rho uw \\ \rho vw \\ \rho w^2 + p \\ (E+p)w \end{pmatrix}_z = 0 \tag{2}$$

where t is the time, (x, y, z) are the spatial coordinates, ρ is the density, $\vec{V} =< u, v, w >$ are the velocities, E is the total energy per unit volume, and p is the pressure. The total energy is the sum of the internal energy and the kinetic energy,

$$E = \rho e + \frac{\rho(u^2 + v^2 + w^2)}{2} \tag{3}$$

where e is the internal energy per unit mass. The two-dimensional Euler equations are obtained by setting $w = 0$, while the one-dimensional Euler equations are obtained by setting both $v = 0$ and $w = 0$.

In general, the pressure can be written as a function of density and internal energy, $p = p(\rho, e)$, or as a function of density and temperature, $p = p(\rho, T)$. In order to complete the model, we need an expression for the internal energy per unit mass. Since $e = e(\rho, T)$ we write

$$de = \left(\frac{\partial e}{\partial \rho}\right)_T d\rho + \left(\frac{\partial e}{\partial T}\right)_\rho dT \tag{4}$$

which can be shown to be equivalent to

$$de = \left(\frac{p - T p_T}{\rho^2}\right) d\rho + c_v dT \tag{5}$$

where c_v is the specific heat at constant volume. [2]

The sound speeds associated with the equations depend on the partial derivatives of the pressure, either p_ρ and p_e or p_ρ and p_T, where the change of variables from density and internal energy to density and temperature is governed by the following relations

$$p_\rho \rightarrow p_\rho - \left(\frac{p - T p_T}{c_v \rho^2} \right) p_T \tag{6}$$

$$p_e \rightarrow p_\rho + \left(\frac{1}{c_v} \right) p_T \tag{7}$$

and the sound speed c is given by

$$c = \sqrt{p_\rho + \frac{p p_e}{\rho^2}} \tag{8}$$

for the case where $p = p(\rho, e)$ and

$$c = \sqrt{p_\rho + \frac{T (p_T)^2}{c_v \rho^2}} \tag{9}$$

for the case where $p = p(\rho, T)$.

2.1.1 Eigensystem

The spatial part of the Euler equations is discretized with an ENO method [21] which requires the eigensystem listed below. Note that we only list the two dimensional eigensystem, since there are no three dimensional examples in this paper. However, the method works well and it is straightforward to implement in three dimensions as we shall show in a future paper. Once the spatial part of the Euler equations is discretized, we apply TVD Runge-Kutta methods for time integration [21].

The eigenvalues and eigenvectors for the Jacobian matrix of $\vec{F}(\vec{U})$ are obtained by setting $A = 1$ and $B = 0$ in the following formulas, while those for the Jacobian of $\vec{G}(\vec{U})$ are obtained with $A = 0$ and $B = 1$.

The eigenvalues are

$$\lambda^1 = \hat{u} - c, \quad \lambda^2 = \lambda^3 = \hat{u}, \quad \lambda^4 = \hat{u} + c \tag{10}$$

and the eigenvectors are

$$\vec{L}^1 = \left(\frac{b_2}{2} + \frac{\hat{u}}{2c}, -\frac{b_1 u}{2} - \frac{A}{2c}, -\frac{b_1 v}{2} - \frac{B}{2c}, \frac{b_1}{2}\right) \tag{11}$$

$$\vec{L}^2 = (1 - b_2, b_1 u, b_1 v, -b_1) \tag{12}$$

$$\vec{L}^3 = (\hat{v}, B, -A, 0) \tag{13}$$

$$\vec{L}^4 = \left(\frac{b_2}{2} - \frac{\hat{u}}{2c}, -\frac{b_1 u}{2} + \frac{A}{2c}, -\frac{b_1 v}{2} + \frac{B}{2c}, \frac{b_1}{2}\right) \tag{14}$$

$$\vec{R}^1 = \begin{pmatrix} 1 \\ u - Ac \\ v - Bc \\ H - \hat{u}c \end{pmatrix}, \quad \vec{R}^2 = \begin{pmatrix} 1 \\ u \\ v \\ H - \frac{1}{b_1} \end{pmatrix} \tag{15}$$

$$\vec{R}^3 = \begin{pmatrix} 0 \\ B \\ -A \\ -\hat{v} \end{pmatrix}, \quad \vec{R}^4 = \begin{pmatrix} 1 \\ u + Ac \\ v + Bc \\ H + \hat{u}c \end{pmatrix} \tag{16}$$

where

$$q^2 = u^2 + v^2, \quad \hat{u} = Au + Bv, \quad \hat{v} = Av - Bu \tag{17}$$

$$, \ = \frac{p_e}{\rho}, \quad c = \sqrt{p_\rho + \frac{\Gamma p}{\rho}}, \quad H = \frac{E + p}{\rho} \tag{18}$$

$$b_1 = \frac{\cdot}{c^2}, \qquad b_2 = 1 + b_1 q^2 - b_1 H \tag{19}$$

The eigensystem for the one-dimensional Euler equations is obtained by setting $v = 0$.

2.2 Level Set Equation

We use the level set equation

$$\phi_t + \vec{W} \cdot \vec{\bigtriangledown}\phi = 0 \tag{20}$$

to keep track of the interface location as the zero level of ϕ. In this equation, $\vec{W}$ is the level set velocity of the interface. In general ϕ starts out as the signed distance function, is advected by solving equation 20 using the methods in [9], and then is reinitialized using

$$\phi_t + S(\phi_o)\left(|\vec{\bigtriangledown}\phi| - 1\right) = 0 \tag{21}$$

to keep ϕ approximately equal to the distance function (i.e. $|\vec{\bigtriangledown}\phi| = 1$) near the interface where we need additional information. We note that our method allows us to solve equation 20 independently of the Euler equations. That is, equation 20 can be solved directly using the method in [9], and the eigensystem for the Euler equations does not depend on ϕ, since we will be solving only one phase problems with any given eigensystem (see the later sections). For more details on the level set function see [5, 17, 25].

2.3 Equation of State

For an ideal gas $p = \rho RT$ where $R = \frac{R_u}{M}$ is the specific gas constant, with $R_u \approx 8.31451 \frac{J}{molK}$ the universal gas constant and M the molecular weight of the gas. Also valid for an ideal gas is $c_p - c_v = R$ where c_p is the specific heat at constant pressure. Additionally, gamma as the ratio of specific heats $\gamma = \frac{c_p}{c_v}$. [8]

For an ideal gas, equation 5 becomes

$$de = c_v dT \tag{22}$$

and assuming that c_v does not depend on temperature (calorically perfect gas), we integrate to obtain

$$e = e_o + c_v T \tag{23}$$

where e_o is not uniquely determined, and we could choose any value for e at $0K$ (although one needs to use caution when dealing with more than one material to be sure that integration constants are consistent with the heat release in any chemical reactions that occur).

Note that we may write

$$p = \rho RT = \frac{R}{c_v}\rho(e - e_o) = (\gamma - 1)\rho(e - e_o) \tag{24}$$

for use in the eigensystem.

3 The GFM for a Contact Discontinuity

The level set function is used to keep track of the interface. The zero level marks the location of the interface, while the positive values correspond to one fluid and the negative values correspond to the other fluid. Each fluid satisfies the Euler equations as described in the last section with different equations of state for each fluid. Based on the work in [9], the discretization of the level set function can be done independently of the two sets of Euler equations. Besides discretizing equation 20 one needs to discretize two sets of Euler equations. This is done with the help of ghost cells.

Any level set function defines two separate domains for the two separate fluids, i.e. each point corresponds to one fluid or the other. Ghost cells are defined at every point in the computational domain so that each grid point contains the mass, momentum, and energy for the real fluid that exists at that point (according to the sign of the level set function) and a ghost mass, momentum, and energy for the other fluid that does not really exist at that grid point (the fluid from the other side of the interface). Once the ghost cells are defined, one can use standard one-phase methods, e.g. see [21], to update the Euler equations at every grid point for both fluids. Then the level set function is advanced to the next time step, and the sign of the level set function is used to determine which of the two sets of updated fluid values should be used as the real fluid values at each grid point.

Consider a general time integrator for the Euler equations. In general, one constructs right hand sides of the ordinary differential equation for both fluids based on the methods in [21], then the level set function is advanced to the next time level and the sign of the level set function determines which of the two right hand sides to use in the time update for the Euler equations. This can be done for every step and every combination of steps in a multistep method.

Lastly, we note that only a band of 3 to 5 ghost cells on each side of the interface is actually needed by the computational method depending on the stencil and movement of the interface. One can optimize the code accordingly.

3.1 Defining Values at the Ghost Cells

In [5], the GFM was implemented for a contact discontinuity in the Euler equations. It was apparent that the pressure and normal velocity were continuous, while the tangential velocity was continuous in the case of a no-slip boundary condition at the interface but discontinuous for a shear wave. It was also apparent that the entropy was discontinuous.

For variables that are continuous across the interface, the ghost fluid values are set to be equal to the real fluid values each grid point. Since these variables are continuous, this node by node population will implicitly capture the correct interface values of the continuous variables.

Note that the discontinuous variables are governed by a linearly degenerate eigenvalue. Thus, they move with the speed of the interface and information in these variables should not cross the interface. In order to avoid numerical smearing of these variables, one-sided constant extrapolation is used to populate the values in the ghost fluid. Note that the work in [6] shows that one does not have to deal directly with the entropy. There are a few options for the choice of the variable used in extrapolation ranging from density to temperature.

The extrapolation of the discontinuous variables is carried out in the following fashion. Using the level set function, define the unit normal at every grid point as

$$\vec{N} = \frac{\vec{\bigtriangledown}\phi}{|\vec{\bigtriangledown}\phi|} =< n_1, n_2, n_3 > \tag{25}$$

where $\vec{N}$ always points from the negative fluid into the positive fluid. Then solve the advection equation

$$I_t \pm \vec{N} \cdot \vec{\bigtriangledown} I = 0 \tag{26}$$

for each variable I that needs to be extrapolated. The "+" sign is used to populate a ghost fluid in the region where $\phi > 0$ with the values of I from the region where $\phi < 0$, while keeping the real fluid values of I fixed in the region where $\phi < 0$. Likewise, the "-" sign is used to populate a ghost fluid in the region where $\phi < 0$ with the values of I from the region where $\phi > 0$, while keeping the real fluid values of I fixed in the region where $\phi > 0$. This equation only needs to be solved for a few time steps to populate a thin band of ghost cells needed for the numerical method.

Note that the above procedure does not apply an isobaric fix to the cells in the real fluid which border the interface. In order to apply the isobaric

fix, keep the real fluid values of I fixed in the region where $\phi < -\epsilon$ when using the "+" sign in equation 26, and keep the real fluid values of I fixed in the region where $\phi > \epsilon$ when using the "-" sign in equation 26. Since ϕ is an approximate distance function, choose ϵ to be the thickness of the band in which the isobaric fix is to be applied. We use $\epsilon = 1.5\triangle x$.

When the need arises to extrapolate the tangential velocity, first extrapolate the entire velocity field, $\vec{V} =< u, v, w >$. Then, at every cell in the ghost region there are two separate velocity fields, one from the real fluid and one from the extrapolated fluid. For each velocity field, the normal component of velocity, $V_N = \vec{V} \cdot \vec{N}$, is put into a three component vector, $V_N \vec{N}$, and then a basis free projection method (see e.g. [7]) is used to define the two dimensional velocity field in the tangent plane by another three component vector, $\vec{V} - V_N \vec{N}$. Finally, the normal component of velocity, $V_N \vec{N}$, from the real fluid is added to the tangential component of velocity, $\vec{V} - V_N \vec{N}$, from the extrapolated fluid to get the ghost fluid velocity that occupies the ghost cell.

Once the ghost fluid values are defined as outlined above, they can be use to assemble the conserved variables for the ghost fluid.

4 Extending the Ghost Fluid Method

For a simple contact discontinuity that moves with the speed of the fluid only, we were able to separate the variables into two sets based on their continuity at the interface. The continuous variables were copied into the ghost fluid in a node by node fashion in order to capture the correct interface values. The discontinuous variables were extrapolated in a one-sided fashion to avoid errors due to numerical dissipation. We wish to apply this idea to a general interface moving at speed D in the normal direction. That is, we need to determine which variables are continuous for this more general problem.

Conservation of mass, momentum, and energy can be applied to an interface in order to abstract continuous variables. One can place a flux on the interface oriented tangent to the interface so that material that passes through this flux passes through the interface. Then this flux will move with speed D (the interface speed) in the normal direction, and the mass, momentum, and energy which flows into this flux from one side of the interface must flow back out the other side of the interface. That is, the mass, momentum, and energy flux in this moving reference frame are continuous variables. Otherwise, there would be a mass, momentum, or energy sink at the interface and conservation would be violated. We denote the mass, momentum, and energy flux in this moving reference frame as F_ρ, $\vec{F}_{\rho\vec{V}}$, and F_E respectively. The statement that these variables are continuous is essentially equivalent to the Rankine-Hugoniot jump conditions at an interface moving with speed D in the normal direction. In [22], [16], [23], and [24] the Rankine-Hugoniot jump conditions were explicitly applied to the interface. We will use the fact that F_ρ, $\vec{F}_{\rho\vec{V}}$, and F_E are continuous to define a ghost fluid that captures the interface values of these variables. That is, we will implicitly capture the Rankine-Hugoniot jump conditions resulting in a method which is robust and easy to implement.

Remark: Note that numerically F_ρ, $\vec{F}_{\rho\vec{V}}$, and F_E may not be continuous. This could occur from initial data or wave interactions. However, since we treat F_ρ, $\vec{F}_{\rho\vec{V}}$, and F_E as though they were continuous in the numerical method, numerical dissipation will smooth them out. In fact, this numerical dissipation will help to guarantee the correct numerical solution.

Remark: The level set function is only designed to represent interfaces

where the interface crosses the material at most once [19, 20]. Simple contact discontinuities that move with the local material velocity never cross over material. If one material is being converted into another then the interface may include a regression rate for this conversion. If the regression rate for this conversion of one material into another is based on some sort of chemical reaction, then the interface can pass over a material exactly once changing it into another material. The same chemical reaction cannot occur to a material more than once.

Remark: Shocks may be interpreted as the conversion of an uncompressed material into a compressed material. In this case, D would be the shock speed. This method could be used to follow a lead shock, but since shocks can pass over a material more than once, all subsequent shocks must be captured. A simple example of the GFM for non-reactive shock waves is presented in a later section, although this approach will be examined in detail in a future paper [1].

Remark: In the general case, $\vec{F}_{\rho\vec{V}}$ and F_E will include general mechanical stress terms on the interface, e.g. viscosity, surface tension, and material models. General mechanical stress terms will be considered in future papers. In this paper, pressure will be the only mechanical stress on the interface.

Remark: In the general case, F_E will include general thermal stress on the interface, e.g. thermal conductivity. Thermal stress will be considered in a future paper.

To define F_ρ, $\vec{F}_{\rho\vec{V}}$, and F_E, the equations are written in conservation form for mass, momentum, and energy. The fluxes for these variables are then rewritten in the reference frame of a flux which is tangent to the interface by simply taking the dot product with the normal direction,

$$\left\langle \vec{F}(\vec{U}), \vec{G}(\vec{U}), \vec{H}(\vec{U}) \right\rangle \cdot \vec{N} = \begin{pmatrix} \rho \\ \rho \vec{V}^T \\ E + p \end{pmatrix} V_N + \begin{pmatrix} 0 \\ p\vec{N}^T \\ 0 \end{pmatrix} \tag{27}$$

where $V_N = \vec{V} \cdot \vec{N}$ is the local fluid velocity normal to the interface and the superscript T designates the transpose. Then the measurements are taken in the moving reference frame (speed D) to get

$$\begin{pmatrix} \rho \\ \rho \left(\vec{V}^T - D\vec{N}^T \right) \\ \rho e + \frac{\rho |\vec{V} - D\vec{N}|^2}{2} + p \end{pmatrix} (V_N - D) + \begin{pmatrix} 0 \\ p\vec{N}^T \\ 0 \end{pmatrix} \tag{28}$$

from which we define

$$F_\rho = \rho(V_N - D) \tag{29}$$

$$\vec{F}_{\rho\vec{V}} = \rho\left(\vec{V}^T - D\vec{N}^T\right)(V_N - D) + p\vec{N}^T \tag{30}$$

$$F_E = \left(\rho e + \frac{\rho|\vec{V} - D\vec{N}|^2}{2} + p\right)(V_N - D) \tag{31}$$

as continuous variables for use in the GFM. That is, we will define the ghost fluid in a node by node fashion by solving the system of equations

$$F_\rho^G = F_\rho^R \tag{32}$$

$$\vec{F}_{\rho\vec{V}}^G = \vec{F}_{\rho\vec{V}}^R \tag{33}$$

$$F_E^G = F_E^R \tag{34}$$

at each grid point. Note that the superscript "R" stands for a real fluid value at a grid point, while the superscript "G" stands for a ghost fluid value at a grid point. Since F_ρ^R, $\vec{F}_{\rho\vec{v}}^R$, F_E^R, $\vec{N}$, and D are known at each grid point, these can be substituted into equations 32, 33, and 34, leaving ρ^G, $\vec{V}^G$, p^G, and e^G undetermined. Since the ghost fluid is supposed to represent the real fluid on the other side of the interface, we use that fluid's equation of state as our sixth equation. Thus, populating the ghost nodes requires the solution of six algebraic equations with six unknowns at each grid point. For many applications, this is rather trivial compared to applying the Rankine-Hugoniot jump conditions explicitly to the interface.

5 Defining the interface speed D

The interface speed is usually a function of the surrounding materials. For example, in the case of a simple contact discontinuity, D can be defined as the continuous normal velocity of the two materials at the interface.

In order to update equation 20 for the level set function, one needs to define the level set velocity, $\vec{W}$, at every grid point. In the level set capturing framework, $\vec{W}$ is defined everywhere by a function which is continuous in the normal direction and has an interface value that moves the interface at the correct interface velocity. This global definition of $\vec{W}$ is the one we use to find D for use in solving equations 32, 33, and 34. In a node by node fashion, we define $D = \vec{W} \cdot \vec{N}$ as the velocity of the interface in the normal direction, capturing the correct value of D at the interface.

In many cases, D is given and we need to define $\vec{W}$. In these instances, we define $\vec{W} = D\vec{N}$. It is interesting to note that if we start with $\vec{W}$, define $D = \vec{W} \cdot \vec{N}$ and then define $\vec{W} = D\vec{N}$, the final result is $\vec{W} = \vec{W}\vec{N}^T\vec{N}$ where the superscript T represents the transpose. While this equation is obviously false, both $\vec{W}$ and $\vec{W}\vec{N}^T\vec{N}$ behave the same in regards to the level set method. That is,

$$\phi_t + \vec{W} \cdot \vec{\bigtriangledown}\phi = 0 \tag{35}$$

and

$$\phi_t + (\vec{W}\vec{N}^T\vec{N}) \cdot \vec{\bigtriangledown}\phi = 0 \tag{36}$$

will be analytically equivalent, although there may be slight numerical differences.

5.1 A simple contact discontinuity

Consider the case of a simple contact discontinuity where the interface moves with the local fluid velocity, i.e. $\vec{W} = \vec{V}$. Then $D = V_N^R$ is the component of the real fluid velocity normal to the interface at each point. Equation 32 becomes,

$$\rho^G(V_N^G - V_N^R) = 0 \tag{37}$$

implying that $V_N^G = V_N^R$. That is, the normal component of the ghost fluid velocity should be equal to the normal component of the real fluid velocity at each point. Then equation 33 becomes $p^G = p^R$ implying that the pressure of the ghost fluid should be equal to the pressure of the real fluid at each point. Equation 34 is then trivially satisfied and we are left with some freedom. As shown earlier, the entropy should be extrapolated in the normal direction along with an Isobaric Fix [6] to minimize "overheating". The tangential velocities may be extrapolated for a shear wave or copied over node by node to enforce continuity of the tangential velocities for a "no-slip" boundary condition.

5.2 Defining the level set velocity $\vec{W}$

One issue that needs to be addressed in the level set formulation is how to define the level set velocity $\vec{W}$ for use in equation 20. In the case of a simple contact discontinuity, $\vec{W} = \vec{V}$ is just the local fluid velocity. In more general cases, the interface speed may be a function of the variables on both sides of the interface and a general method for constructing $\vec{W}$ is needed.

Suppose that we have an interface which separates two materials with states represented by $\vec{U}^{(1)}$ on one side of the interface and $\vec{U}^{(2)}$ on the other side of the interface. In general, the velocity of the interface can be defined by $\vec{W} = \vec{W}(\vec{U}_{int}^{(1)}, \vec{U}_{int}^{(2)})$ where the "int" subscript represents a variable that has been interpolated to the interface in a one-sided fashion. Generally, $\vec{W}$ is a continuous function and application of $\vec{W} = \vec{W}(\vec{U}^{(1)}, \vec{U}^{(2)})$ in a node by node fashion will capture the correct value of $\vec{W}$ at the interface.

In order to apply $\vec{W} = \vec{W}(\vec{U}^{(1)}, \vec{U}^{(2)})$ in a node by node fashion, we need values of $\vec{U}^{(1)}$ and $\vec{U}^{(2)}$ at every node. This means that we need to extend $\vec{U}^{(1)}$ across the interface into the region occupied by $\vec{U}^{(2)}$, and we need to extend $\vec{U}^{(2)}$ across the interface into the region occupied by $\vec{U}^{(1)}$. In this way, we will have values of $\vec{U}^{(1)}$ and $\vec{U}^{(2)}$ at every grid point for use in defining $\vec{W}$.

For first order accuracy, we use constant extension which is governed by the advection equation,

$$I_t \pm \vec{N} \cdot \vec{\bigtriangledown} I = 0 \tag{38}$$

for each variable I that we wish to extrapolate. The "$\pm$" sign is chosen in the appropriate way to extend the components of $\vec{U}^{(1)}$ or of $\vec{U}^{(2)}$.

In general, one only needs extension for a thin band consisting of a few grid cells near the interface. Once the velocity is computed near the interface, it can be extended to cover the entire domain using equation 38 with I equal to each component of $\vec{W}$ and the appropriate choices of the "$\pm$" sign.

In some cases, we prefer to work with D instead of $\vec{W}$. We apply $\vec{D} = \vec{D}(\vec{U}_{int}^{(1)}, \vec{U}_{int}^{(2)})$ in a node by node fashion and then construct $\vec{W} = D\vec{N}$.

6 Examples

Suppose that we have an interface which separates two materials with states represented by $\vec{U}^{(1)}$ on one side of the interface and $\vec{U}^{(2)}$ on the other side of the interface. We use equation 38 to extend $\vec{U}^{(1)}$ and $\vec{U}^{(2)}$ so that both functions are defined on a band near the interface.

Once $\vec{U}^{(1)}$ and $\vec{U}^{(2)}$ are defined at each point near the interface, we apply $D = (\vec{U}^{(1)}, \vec{U}^{(2)})$ in a node by node fashion near the interface. Then we define $\vec{W} = D\vec{N}$ in a node by node fashion near the interface and extend the components of $\vec{W}$ using equation 38 in order to define $\vec{W}$ everywhere. In fact, in the sense of a local level set method, we only need $\vec{W}$ near the interface and it may be taken to be zero elsewhere.

Note that all our numerical examples use third order TVD Runge-Kutta and third order ENO-LLF [21].

6.1 Non-Reacting Shocks

We represent a lead shock by a level set function where the positive values of ϕ correspond to unshocked material and the negative values of ϕ correspond to the shocked material. Then the normal, $\vec{N}$, points from the shocked material into the unshocked material.

In one spatial dimension, the normal velocity is defined as $V_N = u\vec{N}$ and equations 29, 30, and 31 become

$$F_\rho = \rho(V_N - D) \tag{39}$$

$$\vec{F}_{\rho\vec{V}} = \rho(u - D\vec{N}^T)(V_N - D) + p\vec{N}^T \tag{40}$$

$$F_E = \left(\rho e + \frac{\rho|u - D\vec{N}|^2}{2} + p\right)(V_N - D) \tag{41}$$

where we find it useful to define

$$F_{\rho\vec{V}_N} = \vec{N}\vec{F}_{\rho\vec{V}} = \rho(V_N - D)^2 + p \tag{42}$$

and to rewrite equation 41 as

$$F_E = \left(\rho e + \frac{\rho (V_N - D)^2}{2} + p \right) (V_N - D) \tag{43}$$

using the fact that $\vec{N} = \pm 1$ in one dimension. This allows us to write equations 32, 33, and 34 as

$$\rho^G (V_N^G - D) = F_\rho^R \tag{44}$$

$$\rho^G (V_N^G - D)^2 + p^G = F_{\rho \vec{V}_N}^R \tag{45}$$

$$\left(\rho^G e^G + \frac{\rho^G (V_N^G - D)^2}{2} + p^G \right) (V_N^G - D) = F_E^R \tag{46}$$

where F_ρ^R, $F_{\rho \vec{V}_N}^R$, F_E^R, and D can be evaluated at each grid point. If we add the equation of state for the ghost fluid as

$$p^G = (\gamma^G - 1) \rho^G e^G \tag{47}$$

we can solve four equations in four unknowns which we arrange into a quadratic for $V_N^G - D$ and solve to get

$$V_N^G - D = \frac{\gamma^G F_{\rho \vec{V}_N}^R}{(\gamma^G + 1) F_\rho^R} \pm \sqrt{\left(\frac{\gamma^G F_{\rho \vec{V}_N}^R}{(\gamma^G + 1) F_\rho^R} \right)^2 - \frac{2(\gamma^G - 1) F_E^R}{(\gamma^G + 1) F_\rho^R}} \tag{48}$$

as our two solutions. Once we decide which of the two solutions for V_N^G to use, we use equation 44 to find ρ^G, equation 45 to find p^G, and equation 47 to find e^G. In addition, we have $u^G = V_N^G \vec{N}$.

In order to choose the correct solution from equation 48, one has to know whether or not the ghost fluid is an unshocked fluid or a shocked fluid. Node by node, the real values of the unshocked fluid are used to create a shocked ghost fluid to help in the discretization of the shocked real fluid. Likewise, the real values of the shocked fluid are used to create an unshocked ghost fluid to help in the discretization of the unshocked real fluid. If the ghost fluid is a shocked fluid, then we want D to be subsonic relative to the flow, i.e. $V_N^G - c^G < D < V_N^G + c^G$ or $|V_N^G - D| < c^G$. On the other hand, if the ghost fluid is an unshocked fluid, then we want D to be supersonic relative

to the flow, i.e. $|V_N^G - D| > c^G$. Based on this discussion, we choose the "$\pm$" sign in equation 48 to give the minimum value of $|V_N^G - D|$ when constructing a shocked ghost fluid and the maximum value of $|V_N^G - D|$ when constructing an unshocked ghost fluid.

For a simple non-reacting shock, we may define the shock speed D directly from the mass balance equation as

$$D = \frac{\rho^{(1)} u^{(1)} - \rho^{(2)} u^{(2)}}{\rho^{(1)} - \rho^{(2)}} \tag{49}$$

in a node by node fashion. However, this simple definition of the shock speed will erroneously give $D = 0$ in the case of a standard shock tube problem where both fluids are initially at rest. A somewhat better estimate of the shock speed can be derived by combining equation 49 with the momentum balance equation to get

$$D = \sqrt{\frac{\rho^{(1)} \left(u^{(1)}\right)^2 + p^{(1)} - \rho^{(2)} \left(u^{(2)}\right)^2 - p^{(2)}}{\rho^{(1)} - \rho^{(2)}}} \tag{50}$$

where the shock speed is now dependent on the pressure as well.

Note that equations 49 and 50 are approximations for D. Clearly, these approximations will lead to nonphysical values of D in certain situations. In fact, D could be infinite or imaginary. A more robust, but still approximate value for D can be obtained by evaluating $D = V_N + c$ with the Roe average of $\vec{U}^{(1)}$ and $\vec{U}^{(2)}$, since this is the exact shock speed for an isolated shock wave and never becomes ill-defined. Of course, the best definition of the shock speed can be derived by solving the Riemann problem for the states $\vec{U}^{(1)}$ and $\vec{U}^{(2)}$, although this generally requires an iteration procedure (this approach will be followed in a future paper [1]).

6.1.1 Example 1

In this example, a single shock wave moving to the right is taken from [24]. We use a $1m$ domain with 100 grid points and the interface located at $x = .5m$ which is exactly in between the 50th and 51st grid points. We use $\gamma = 1.4$ and $M = .040\frac{kg}{mol}$ for both gases. Initially, we set $\rho = 2.124\frac{kg}{m^3}$, $u = 89.981\frac{m}{s}$, and $p = 148407.3Pa$ on the left, and $\rho = 1.58317\frac{kg}{m^3}$, $u = 0\frac{m}{s}$, and $p = 98066.5Pa$ on the right. Figure 1 shows the solution at $t = .001s$ with a standard shock capturing scheme. Note that the standard scheme

smears out this perfect shock and creates numerical artifacts in the process, e.g. there is a glitch near $x = .6$ in the density and temperature.

Figure 2 shows the numerical solution computed with equation 50 as the shock speed for the GFM. Note that the GFM avoids numerical dissipation at the interface and the related artifacts.

The exact solution is plotted as a solid line in both figures.

6.1.2 Example 2

Next, we set up a shock tube problem by changing the left state in example 1 to $\rho = 3\frac{kg}{m^3}$, $u = 0\frac{m}{s}$, and $p = 2 \times 10^5 Pa$ while still plotting the results at $t = .001s$. The results with a standard shock capturing scheme are shown in figure 3 and those with the GFM and equation 50 are shown in figure 4. Note that the small glitch on the left hand side of the shock disappears when the shock speed equilibrates later in time. In addition, a more resolved calculation will achieve a flat profile in a shorter time, e.g. the same calculation with 400 grid points has no visible glitch as can be seen in figure 5. We also note that convergence to the exact Riemann solution was observed upon grid refinement. The exact solution is plotted as a solid line in all 3 figures.

6.2 Detonations

Strong detonations and Chapman-Jouguet detonations can be approximated as reacting shocks under the assumption that the reaction zone has negligible thickness. We represent the unreacted material with positive values of ϕ and the reacted material with negative values of ϕ. Then the normal, $\vec{N}$, points from the reacted material into the unreacted material.

Equations 44, 45, and 46 are still valid, while equation 47 becomes

$$p^G = (\gamma^G - 1)\rho^G(e^G - e_o^G) \tag{51}$$

where we can no longer set $e_o = 0$ for both fluids. In detonations, the jump in e_o across the reaction front indicates the energy release in the chemical reaction.

Equation 48 becomes

$$V_N^G - D = \frac{\gamma^G F^R_{\rho\vec{V}_N}}{(\gamma^G + 1)F_\rho^R} \pm \sqrt{\left(\frac{\gamma^G F^R_{\rho\vec{V}_N}}{(\gamma^G + 1)F_\rho^R}\right)^2 - \frac{2(\gamma^G - 1)}{(\gamma^G + 1)}\left(\frac{F_E^R}{F_\rho^R} - e_o^G\right)} \tag{52}$$

where we choose the "$\pm$" sign to give the minimum value of $|V_N^G - D|$ when constructing a reacted ghost fluid and the maximum value of $|V_N^G - D|$ when constructing an unreacted ghost fluid.

We use equation 50 for the detonation speed D, although one may wish to consult a Riemann solver, e.g. see [26].

6.2.1 Example 3

In this example, a single overdriven detonation wave moving to the right is taken from [16]. We use an $8m$ domain with 100 grid points and the interface located at $x = 4m$ which is exactly in between the 50th and 51st grid points. We use $\gamma = 1.27$ in both gases, while $M = .015\frac{kg}{mol}$ in the unburnt gas and $M = .018\frac{kg}{mol}$ in the burnt gas. Initially, we set $\rho = 1.57861\frac{kg}{m^3}$, $u = 2799.82\frac{m}{s}$, and $p = 7707520Pa$ on the left, and $\rho = .601\frac{kg}{m^3}$, $u = 0\frac{m}{s}$, and $p = 1 \times 10^5 Pa$ on the right. In addition, we have $e_o = \frac{242000}{.018}\frac{J}{kg}$ in the unburnt gas and $e_o = 0$ in the burnt gas. Figure 6 shows the solution at $t = .0005s$ after it has moved from $x = 4m$ to about $x = 6.26m$ at a speed of about $4521\frac{m}{s}$. The exact solution is plotted as a solid line in the figure.

6.2.2 Example 4

Next, we take the overdriven detonation from example 3, increase the resolution of the problem to 800 grid cells (801 grid points), and start the detonation at $x = .175m$ which is exactly between the 18th and 19th gird points. A solid wall boundary condition is enforced at $x = 0$, creating a rarefaction wave that will catch up with the overdriven detonation and weaken it to a Chapman-Jouguet detonation as in [16]. Figure 7 shows the pressure profile at $t = .00135s$ and figure 8 shows a plot of the peak post-detonation pressure at each grid point. Note that the post detonation pressure is approaching the Chapman-Jouguet pressure of $4518507Pa$.

6.3 Deflagrations

For a deflagration, we represent the unreacted material with positive values of ϕ and the reacted material with negative values of ϕ so that the normal points from the reacted material into the unreacted material. We use equations 44, 45, and 46 along with equation 51 where the jump in e_o across the reaction

front indicates the energy release in the chemical reaction. Equation 52 is valid, however, since a deflagration is subsonic we choose the "$\pm$" sign to give the minimum value of $|V_N^G - D|$ for both the reacted and unreacted ghost fluids.

For a deflagration, the Riemann problem is not well posed unless the speed of the deflagration is given [11, 26]. Luckily, there is a large amount of literature on the G-equation for flame discontinuities. The G-equation was originally proposed in [15] and later discussed in [27]. The G-equation represents the flame front as a discontinuity in the same way as the level set method. Thus, one can consult the literature on the G-equation to obtain deflagration speeds for the GFM.

6.3.1 Example 5

In this example, we consider a single deflagration wave moving to the right with the deflagration velocity taken from [11] and [26] as

$$D = V_N^{(2)} + 3.00 \times 10^{-9} \frac{s^3}{m^3} \left(\frac{p^{(2)}}{\rho^{(2)}} \right)^2 \tag{53}$$

where we have redimensionalized the problem. Note that the superscript "(2)" stands for an unburnt gas quantity. We use a $1.6m$ domain with 100 grid points and the interface located at $x = .8m$ which is exactly in between the 50th and 51st grid points. We use $\gamma = 1.4$ and $M = .029 \frac{kg}{mol}$ in both gases. Initially, we set $\rho = .142168 \frac{kg}{m^3}$, $u = -181.018 \frac{m}{s}$, and $p = 94569.5 Pa$ on the left, and $\rho = 1 \frac{kg}{m^3}$, $u = 0 \frac{m}{s}$, and $p = 1 \times 10^5 Pa$ on the right. In addition, we have $e_o = 2.0 \times 10^6 \frac{J}{kg}$ in the unburnt gas and $e_o = 0$ in the burnt gas. Figure 9 shows the solution at $t = .01s$ after it has moved from $x = .8m$ to about $x = 1.1m$ at a speed of about $30.0 \frac{m}{s}$. The exact solution is plotted as a solid line in the figure.

6.3.2 Example 6

Next, we take the deflagration from example 5 and enforce a solid wall boundary condition at $x = 0$. It is important to note that a reflection boundary condition is applied to the level set function too. That is, we start with $\phi = x - .024m$ and after applying the reflection boundary condition we have $\phi = |x| - .024m$ as initial data. This initial data assumes that the entire

domain is unburnt (the right state above), except for a small region near the solid wall which we assume to be burnt (the left state above).

Due to the influence of the solid wall, we initially set the velocity of the burnt state to be identically zero (not $-181.018\frac{m}{s}$). Since the solid wall prevents the deflagration from accelerating the burnt gas to the left, a shock wave forms to the right of the deflagration. This shock wave pre-accelerates the unburnt gas to the right, so that the acceleration of the gas to the left by the deflagration wave is approximately canceled, resulting in a burnt gas velocity near zero as forced by the solid wall.

Figure 10 shows the deflagration wave at $t = .002s$ when it located near $x = .5m$ moving to the right at approximately $278\frac{m}{s}$. Note the captured shock wave near $x = .95m$. In addition, note that the overheating errors in temperature and density at the wall could be minimized with the Isobaric Fix [6].

An important technical detail concerns the treatment of the normal in the burnt region near the wall. There are exactly three burnt points consisting of one at $x = 0$, one to the right of $x = 0$, and a solid wall boundary reflected point just to the left of $x = 0$. The normal $\vec{N}$ will be undefined at $x = 0$ if standard central differencing is used to compute it. Thus, one must be careful when computing $\vec{N}$ with a standard central difference. In these cases we resort to one-sided differencing to compute the normal. In this particular example, essentially equivalent results are obtained regardless of which direction we use to compute the one-sided difference. Inherently, this is a problem with level sets in under-resolved regions since local extrema may occur near the zero level. However, this is only a problem when the extrema are positioned exactly on a grid node which is unusual except for initial data. For our purposes, we address this problem by assigning a normal in an arbitrary direction by choosing one-sided differencing in an arbitrary direction.

6.3.3 Example 7

Once again, we will consider deflagration waves with velocities determined by equation 53. We use a $1.6m$ domain with 801 grid points and a solid wall boundary condition at $x = 0$. Initially, $\phi = |x - .078m| - .003m$ where the three grid points at $x = .076m$, $x = .078m$, and $x = .08m$ designate a burnt gas with $\rho = .2082\frac{kg}{m^3}$, $u = 0\frac{m}{s}$, $p = 140720Pa$, and $e_o = 0$. The rest of the domain is an unburnt gas with $\rho = 1\frac{kg}{m^3}$, $u = 0\frac{m}{s}$, $p = 1 \times 10^5 Pa$, and

$e_o = 2.0 \times 10^6 \frac{J}{kg}$. In both gases, $\gamma = 1.4$ and $M = .029 \frac{kg}{mol}$.

The solution consists of two deflagration waves moving outward from $x = .078m$ (in opposite directions). Since the burnt gas is confined between these deflagrations, it must have a near zero velocity inducing shock waves in front of the deflagrations as can be seen in figure 11 at $t = .000147s$ where the deflagrations are located near $x = .043$ and $x = .113$ and the shocks are located near $x = .01$ and $x = .146$.

The leftgoing shock wave will reflect off the solid wall boundary, change direction, and then intersect the leftgoing deflagration near $x = .02m$ causing it to slow down (although it eventually reaches the wall and burns out). The transmitted shock eventually catches up with the rightgoing deflagration near $x = .175m$ causing it to accelerate to the right. The resulting transmitted shock will eventually overtake the lead rightgoing shock. Figure 12 shows a time history of the location of the deflagration waves and figure 13 shows the pressure at $t = .0022s$.

6.4 Example 8

In this example, we compare our results for shock deflagration interactions with exact solutions from [18] using the deflagration velocity

$$D = V_N^{(2)} + 18.5 \left(\frac{p^{(2)}}{101000 Pa} \right)^{.1} \left(\frac{T^{(2)}}{298K} \right)^{1.721} \frac{m}{s} \tag{54}$$

where the superscript "(2)" stands for an unburnt gas quantity. We use a $1m$ domain with 400 grid points and the interface located at $x = .5m$. We use $\gamma = 1.4$, $M = .021 \frac{kg}{mol}$, and $e_o = 3.38 \times 10^6 \frac{J}{kg}$ in the unburnt gas corresponding to a stoichiometric hydrogen air mixture. We use $\gamma = 1.17$, $M = .026 \frac{kg}{mol}$, and $e_o = 0$ in the burnt gas. The burnt gas is on the left of the interface and the unburnt gas is on the right of the interface.

The first case consists of a leftgoing shock starting at $x = .6m$ with preshock states of $\rho = 1.587 \frac{kg}{m^3}$, $u = 283.2 \frac{m}{s}$, and $p = 249,900 Pa$ on the left, and postshock states of $\rho = 2.128 \frac{kg}{m^3}$, $u = 139.9 \frac{m}{s}$, and $p = 378,200 Pa$ on the right. The burnt gas has initial states of $\rho = .4289 \frac{kg}{m^3}$, $u = 194.8 \frac{m}{s}$, and $p = 244,800 Pa$. The shock hits the deflagration and the collision results in four waves shown in figure 14 at $t = .00065s$ as a shock, contact, deflagration, and rarefaction from left to right. Our method agrees well with the exact solution capturing all waves except the deflagration wave which is tracked with the level set function.

The second case consists of a rightgoing shock starting at $x = .4m$ with postshock states of $\rho = .3809\frac{kg}{m^3}$, $u = 555.1\frac{m}{s}$, and $p = 241,100\,Pa$ on the left, and preshock states of $\rho = .1859\frac{kg}{m^3}$, $u = -61.96\frac{m}{s}$, and $p = 102,700\,Pa$ on the right. The unburnt gas has initial states of $\rho = .8672\frac{kg}{m^3}$, $u = 6.762\frac{m}{s}$, and $p = 103,900\,Pa$. The shock hits the deflagration and the collision results in four waves shown in figure 15 at $t = .0006s$ as a shock, contact, deflagration, and shock from left to right. Our method agrees well with the exact solution capturing all waves except the deflagration wave which is tracked with the level set function.

6.5 Multidimensions

In multidimensions, the normal velocity is defined as $V_N = \vec{V} \cdot \vec{N}$, equation 29 is still

$$F_\rho = \rho(V_N - D) \tag{55}$$

and we can still define

$$F_{\rho\vec{V}_N} = \vec{N}\vec{F}_{\rho\vec{V}} = \rho(V_N - D)^2 + p \tag{56}$$

for use in the method. In addition, we define

$$\vec{F}_{\rho\vec{V}_T} = \frac{\vec{F}_{\rho\vec{V}} - F_{\rho\vec{V}_N}\vec{N}^T}{F_\rho} = \vec{V}^T - V_N\vec{N}^T \tag{57}$$

as a valid expression when $V_N \neq D$ (a contact discontinuity). The necessary continuity of this expression implies the well known fact that tangential velocities are continuous across shocks, detonations, and deflagrations. Note that the tangential velocities are not necessarily continuous across a contact discontinuity.

Next, we write

$$|\vec{V} - D\vec{N}|^2 = |\vec{V}|^2 - 2DV_N + D^2 = |\vec{V}|^2 - V_N^2 + (V_N - D)^2 \tag{58}$$

and define the velocities in the tangent directions T_1 and T_2 as V_{T_1} and V_{T_2} so that we may use

$$|\vec{V}|^2 = V_N^2 + V_{T_1}^2 + V_{T_2}^2 \tag{59}$$

in order to obtain

$$|\vec{V} - D\vec{N}|^2 = V_{T_1}^2 + V_{T_2}^2 + (V_N - D)^2 \tag{60}$$

which is plugged into equation 31 resulting in

$$F_E = \left(\rho e + \frac{\rho(V_{T_1}^2 + V_{T_2}^2)}{2} + \frac{\rho(V_N - D)^2}{2} + p \right) (V_N - D) \tag{61}$$

as a rewritten version of equation 31.

Next we define

$$\hat{F}_E = F_E - \frac{F_\rho(V_{T_1}^2 + V_{T_2}^2)}{2} = \left(\rho e + \frac{\rho(V_N - D)^2}{2} + p \right) (V_N - D) \tag{62}$$

and use this equation along with equation 55, equation 56 and the equation of state for the ghost fluid

$$p^G = (\gamma^G - 1)\rho^G(e^G - e_o^G) \tag{63}$$

to obtain

$$V_N^G - D = \frac{\gamma^G F^R_{\rho\vec{V}_N}}{(\gamma^G + 1)F_\rho^R} \pm \sqrt{\left(\frac{\gamma^G F^R_{\rho\vec{V}_N}}{(\gamma^G + 1)F_\rho^R} \right)^2 - \frac{2(\gamma^G - 1)}{(\gamma^G + 1)} \left(\frac{\hat{F}_E^R}{F_\rho^R} - e_o^G \right)} \tag{64}$$

which is identical to equation 52 in every way, since our definition of $\hat{F}_E$ in multidimensions is identical to the definition of F_E in one-dimension.

To summarize, we use equation 64 to find V_N^G, with the proper choice of the "$\pm$" sign outlined in the one dimensional cases. Then we use equation 55 to find ρ^G, equation 56 to define p^G, and equation 63 to find e^G. The velocity, $\vec{V}^G$ is obtained by combining the normal velocity of the ghost fluid with the tangential velocity of the real fluid through the equation

$$\vec{V}^G = V_N^G \vec{N} + \vec{V}^R - V_N^R \vec{N} \tag{65}$$

where $V_N^R = \vec{V}^R \cdot \vec{N}$ is the normal velocity of the real fluid. Note that we never use the tangent directions so that the method is simple to apply in three dimensions.

6.6 Example 9

This problem is similar to the example in section 5.1 of [24]. Consider a $1m$ square domain with 100 grid cells in each direction. Two circular regions of burnt gas are centered at $(.425m, .425m)$ and at $(.575m, .575m)$ with a radius of $.02m$ each. The rest of the domain is defined as unburnt gas. Both the burnt gas and the unburnt gas are defined as in example 5, except we set $u = v = 0\frac{m}{s}$ in the burnt gas similar to example 6.

In each circular region, a shock wave will form and travel outward pre-accelerating the unburnt gas similar to the one-dimensional result calculated in example 6. Since there are two circular regions, these shock waves will intersect each other and interfere with the circular growth of the burnt regions distorting their shape. Figure 16 and figure 17 show the interface locations before and after merging corresponding to .0008 seconds and .001 seconds, respectively.

In figure 18 and figure 19 we plot square cells which are color coded based on the density values at the cell centers. A color bar is included to the right of each figure to illustrate the discontinuous density profile at the interface. The density jumps more than $1\frac{kg}{m^3}$ without the presence of intermediate values due to numerical dissipation. Note that the "white" region away from the interface is due to shock wave compressions.

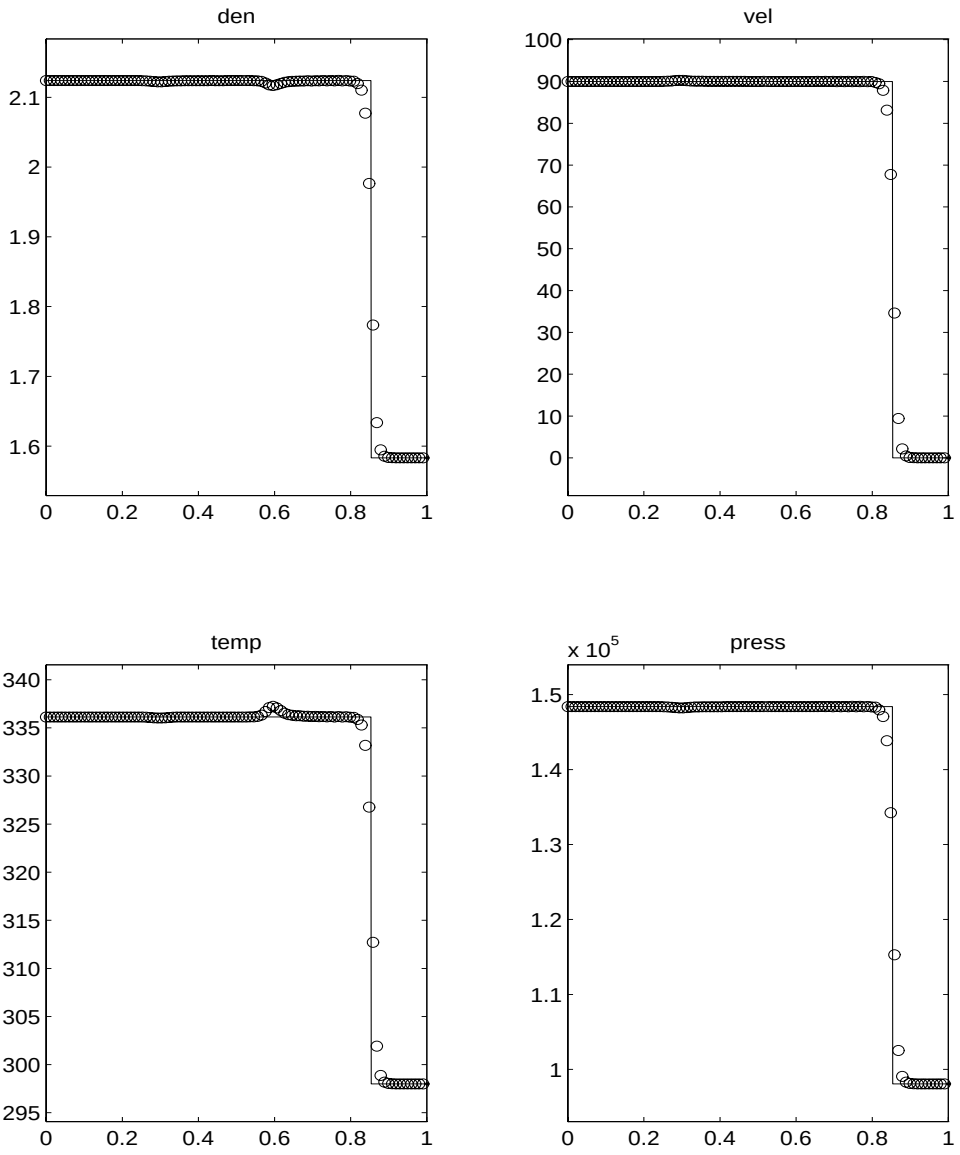

Figure 1: Single Shock (Standard Shock Capturing Scheme)

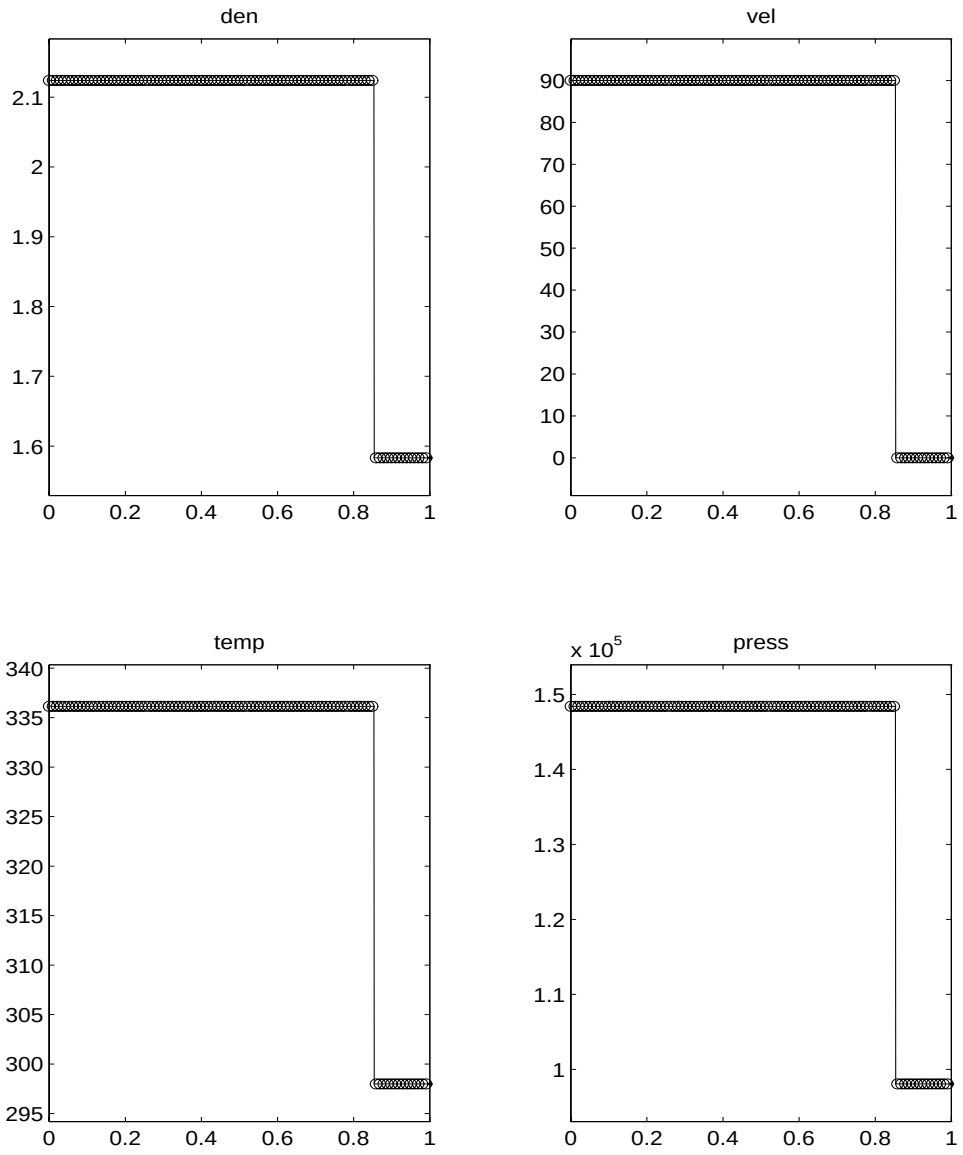

Figure 2: Single Shock (Ghost Fluid Method)

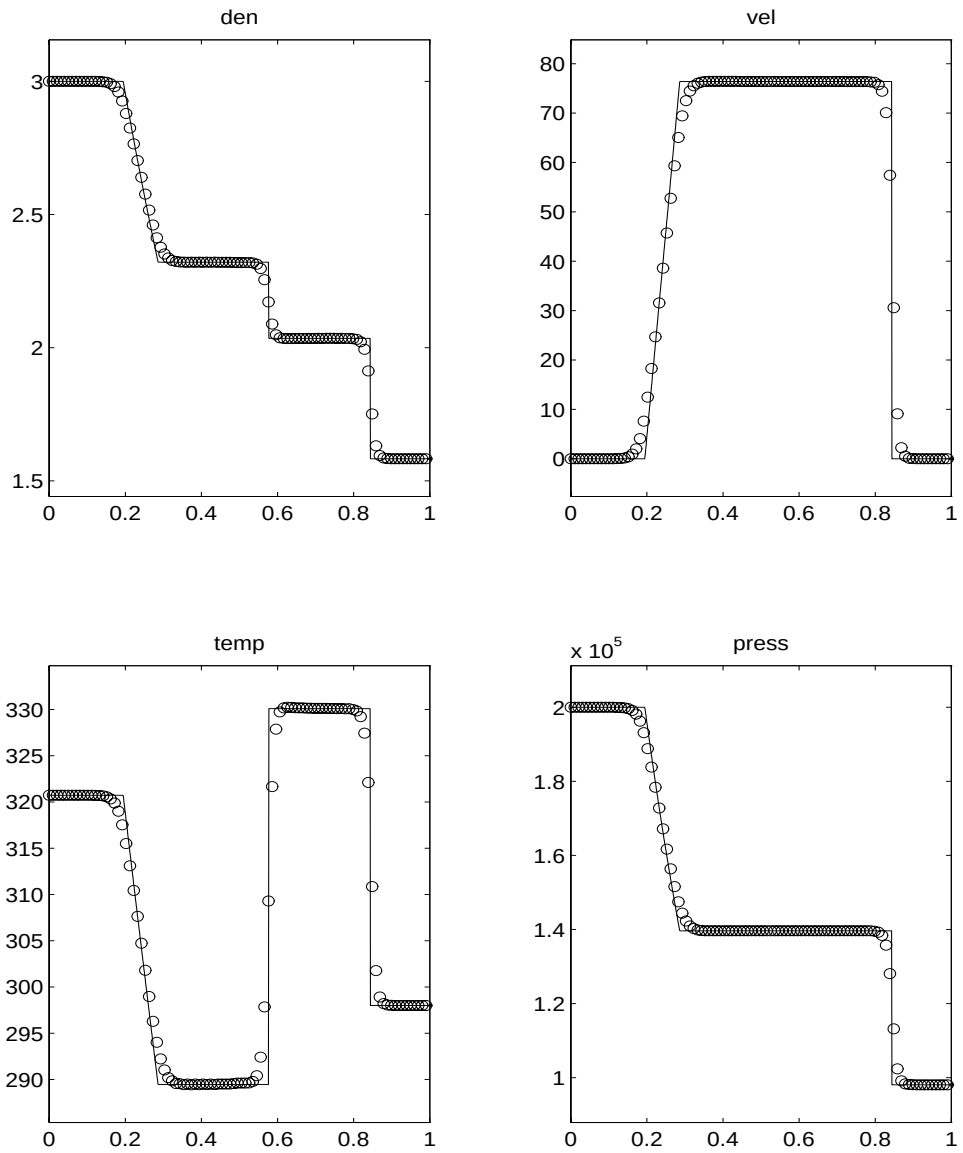

Figure 3: Shock Tube (Standard Shock Capturing Scheme) - 100 grid points

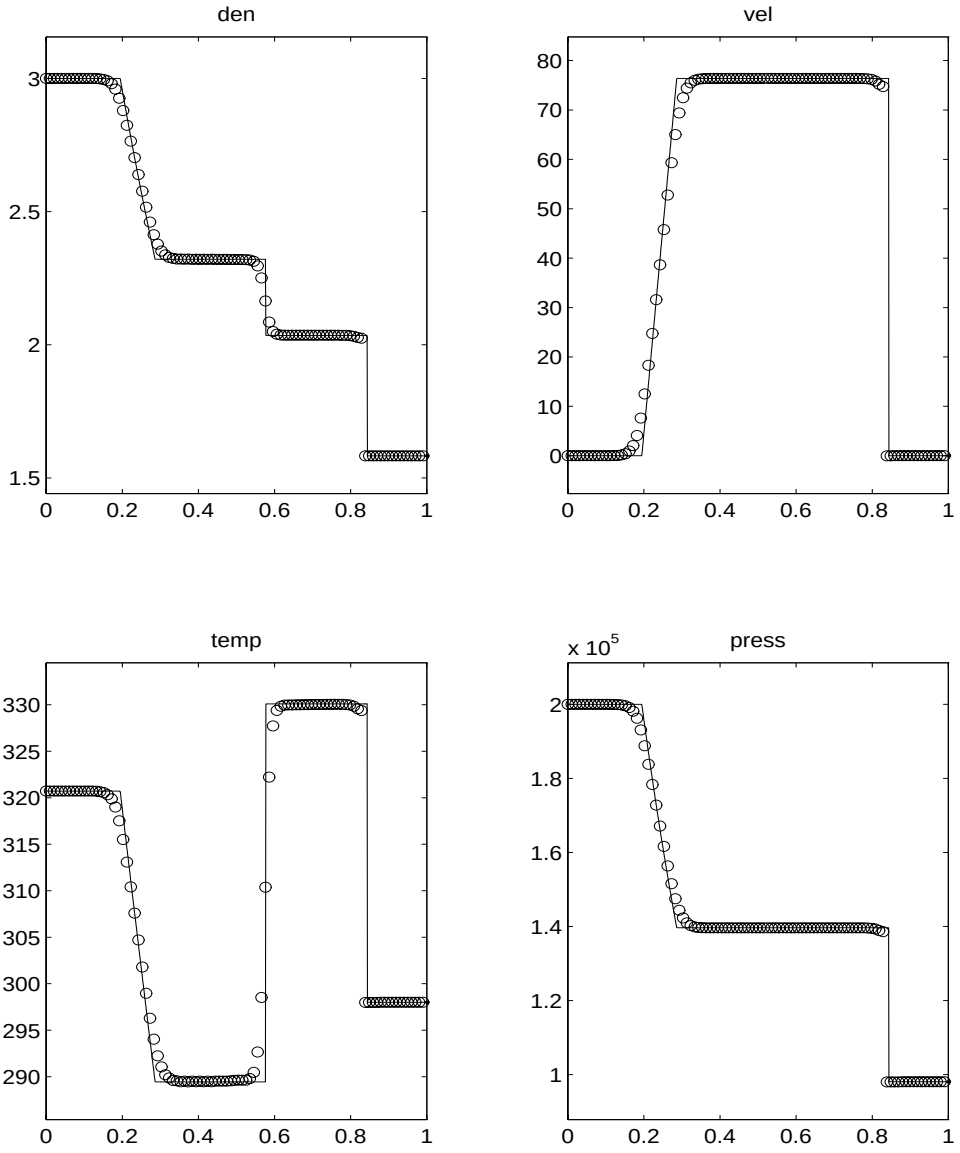

Figure 4: Shock Tube (Ghost Fluid Method) - 100 grid points

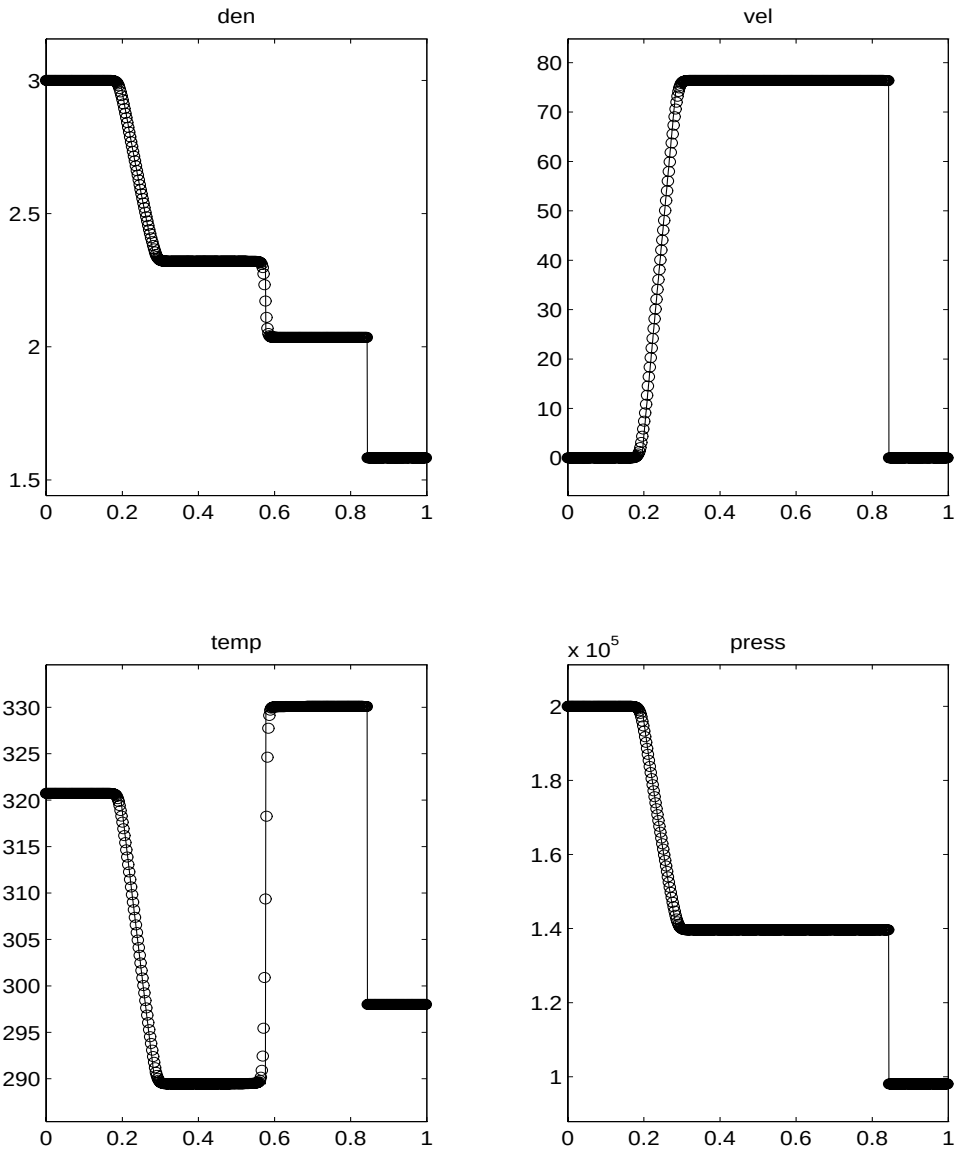

Figure 5: Shock Tube (Ghost Fluid Method) - 400 grid points

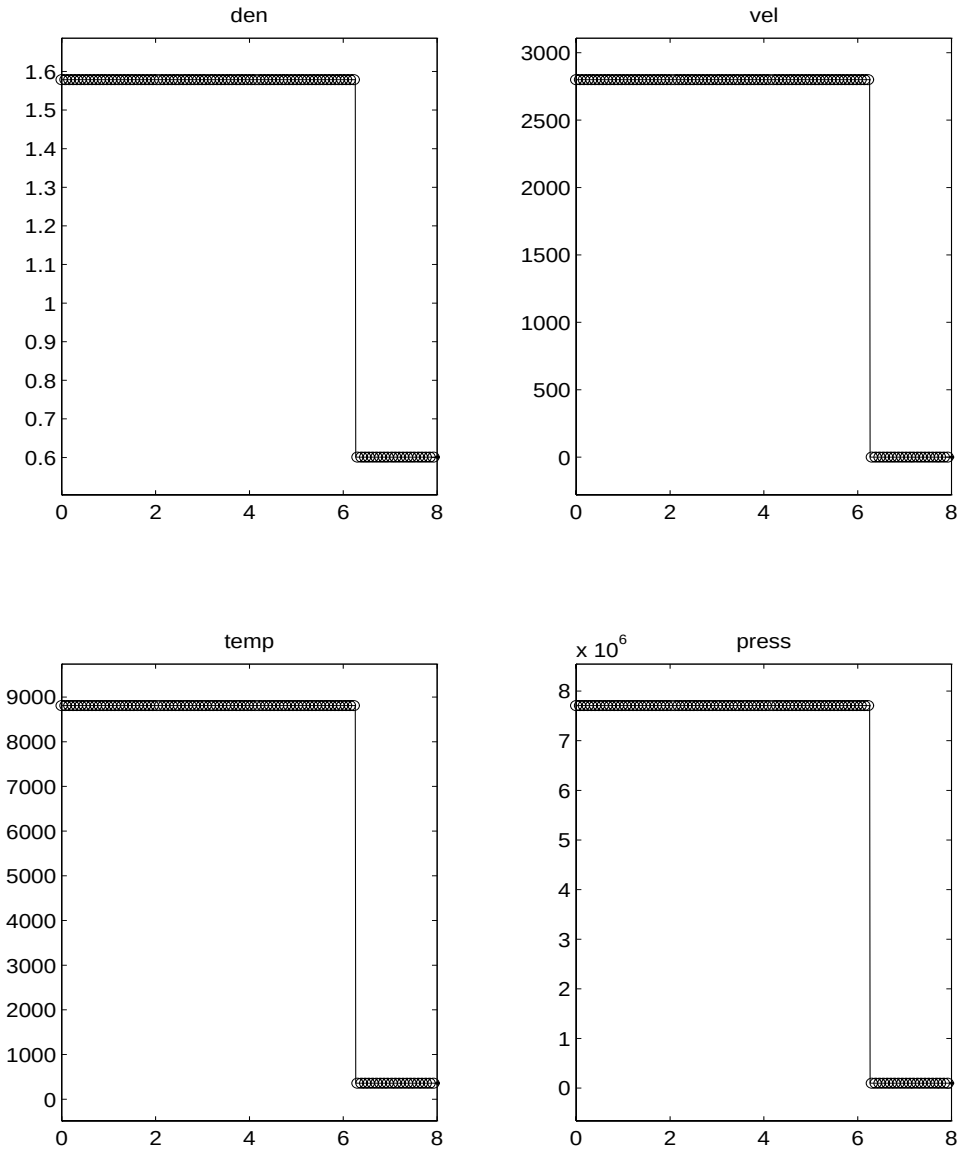

Figure 6: Overdriven Detonation

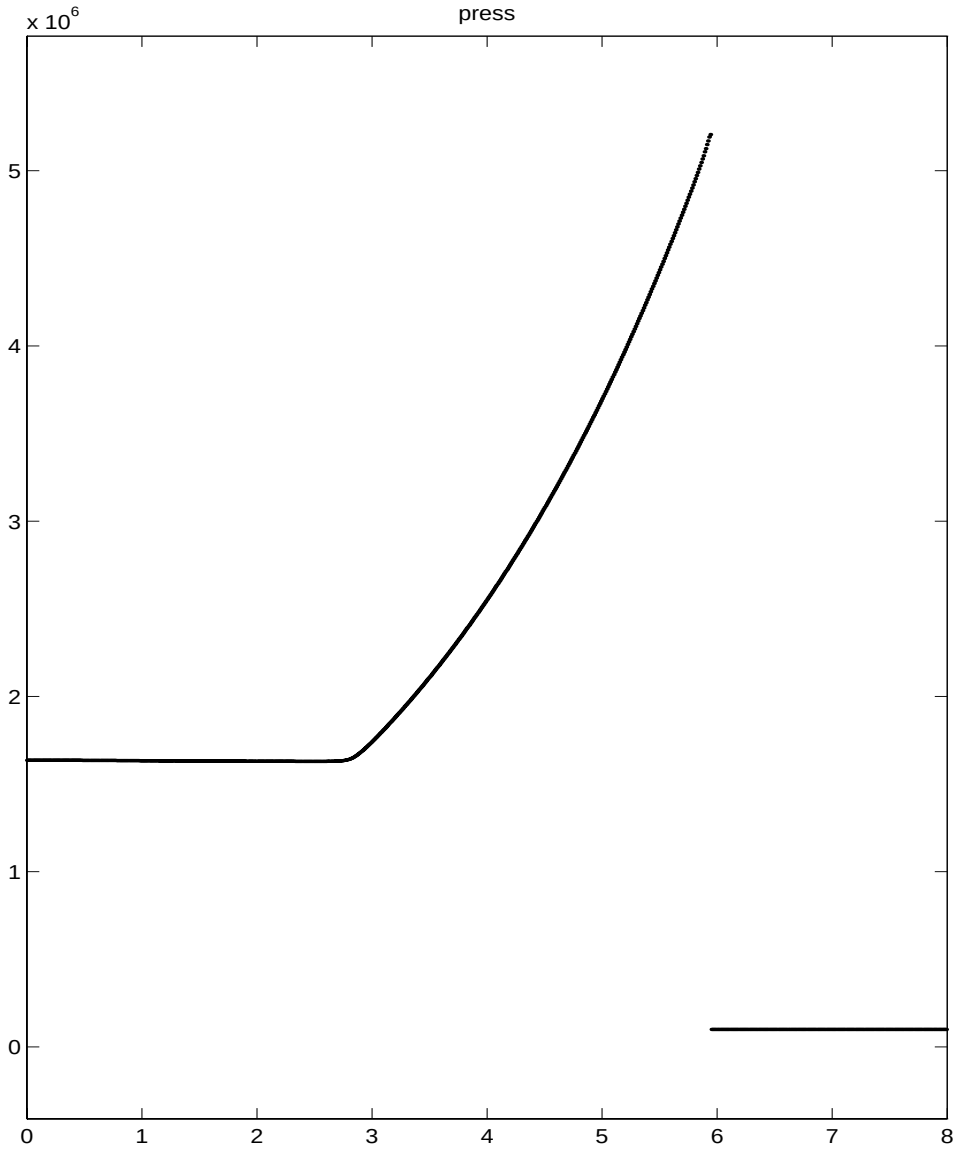

Figure 7: Overdriven Detonation at $t = .00135s$

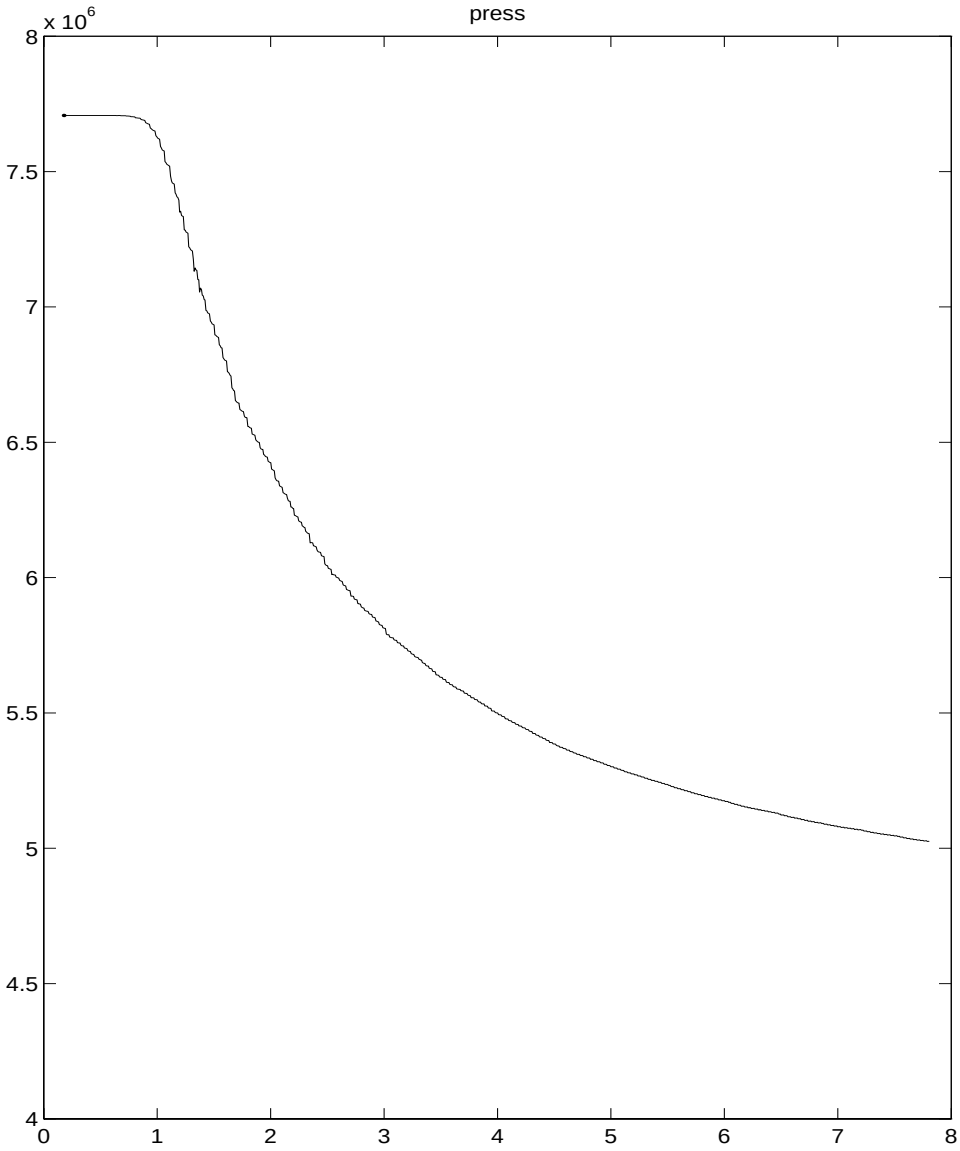

Figure 8: Spatial History of the Peak Pressure

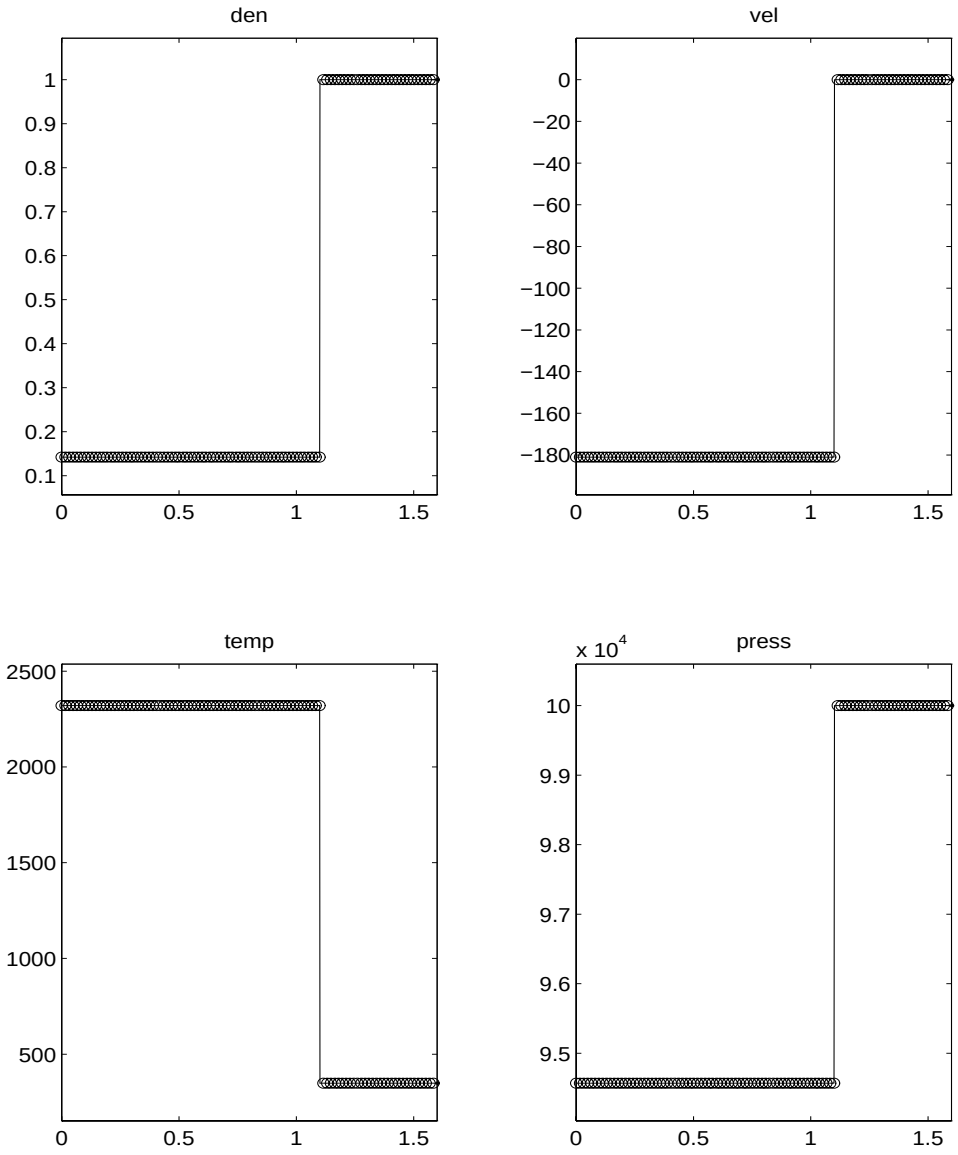

Figure 9: Deflagration Wave

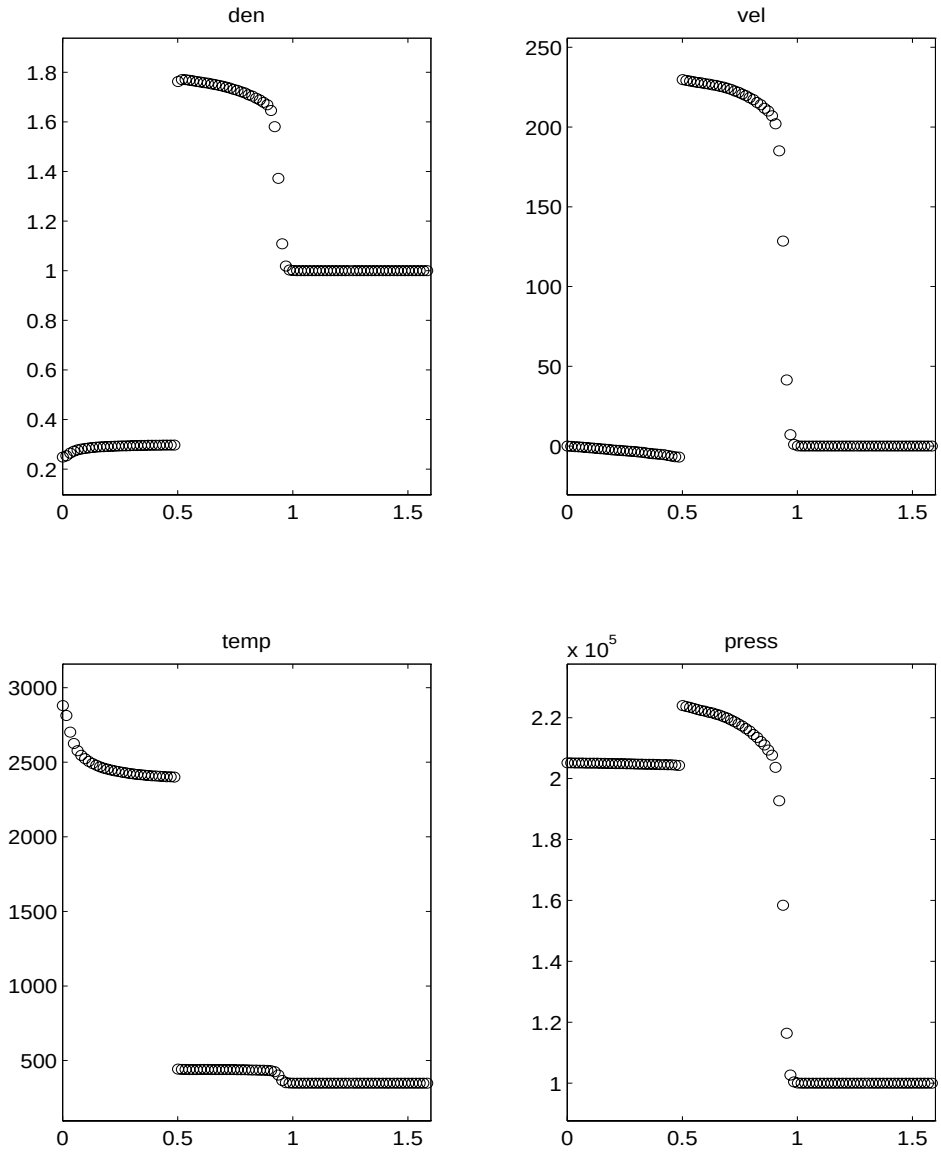

Figure 10: Deflagration Wave with a Precursor Shock Wave

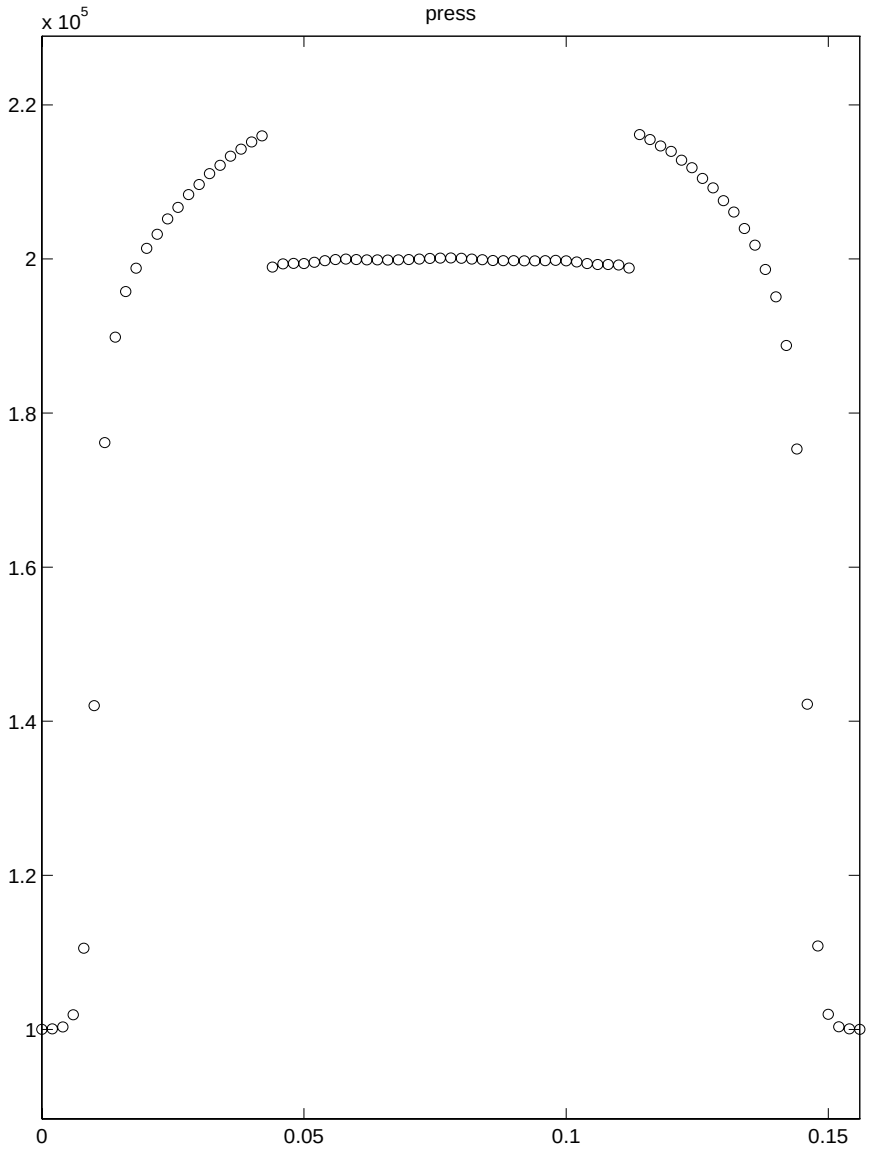

Figure 11: Deflagration Waves with Precursor Shock Waves

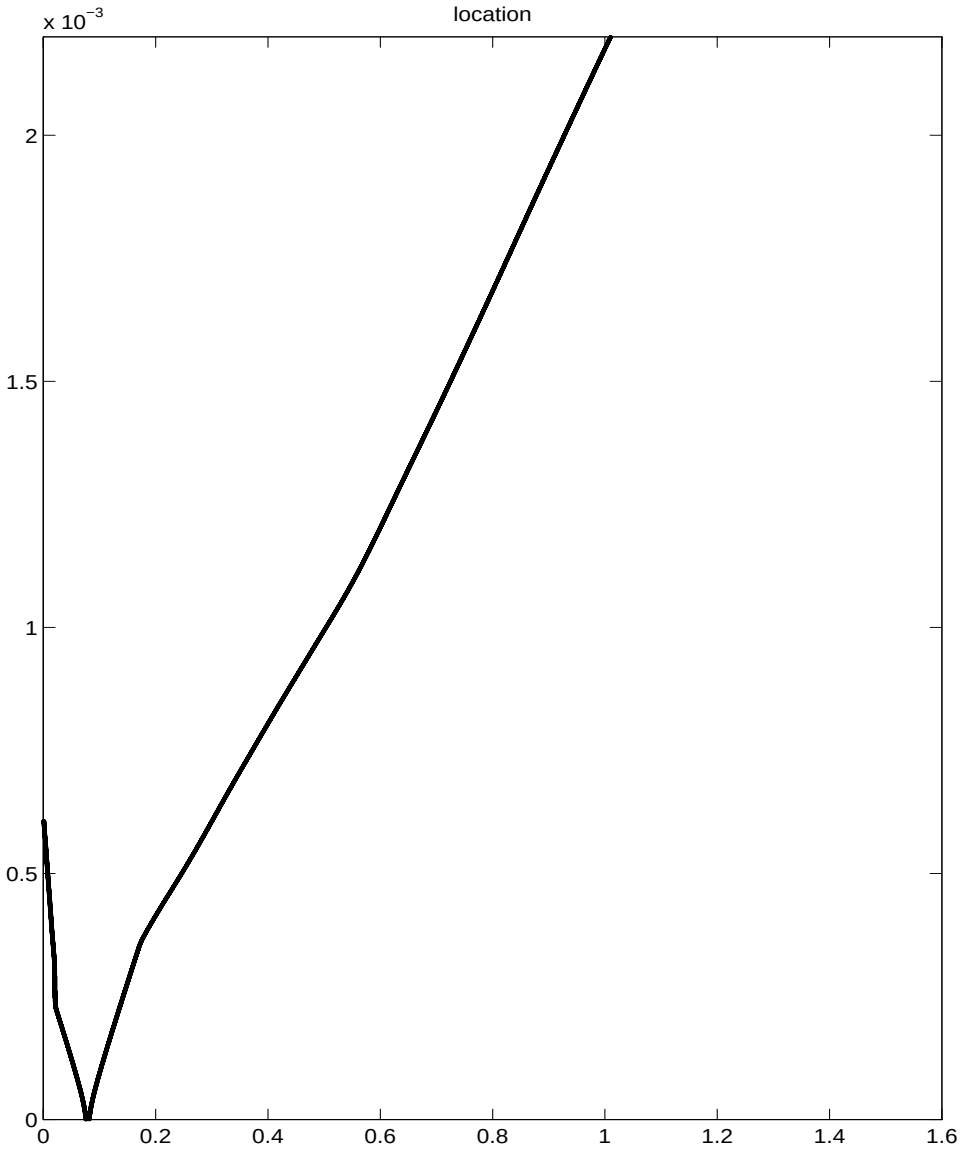

Figure 12: Deflagration Wave Location (time vs. space)

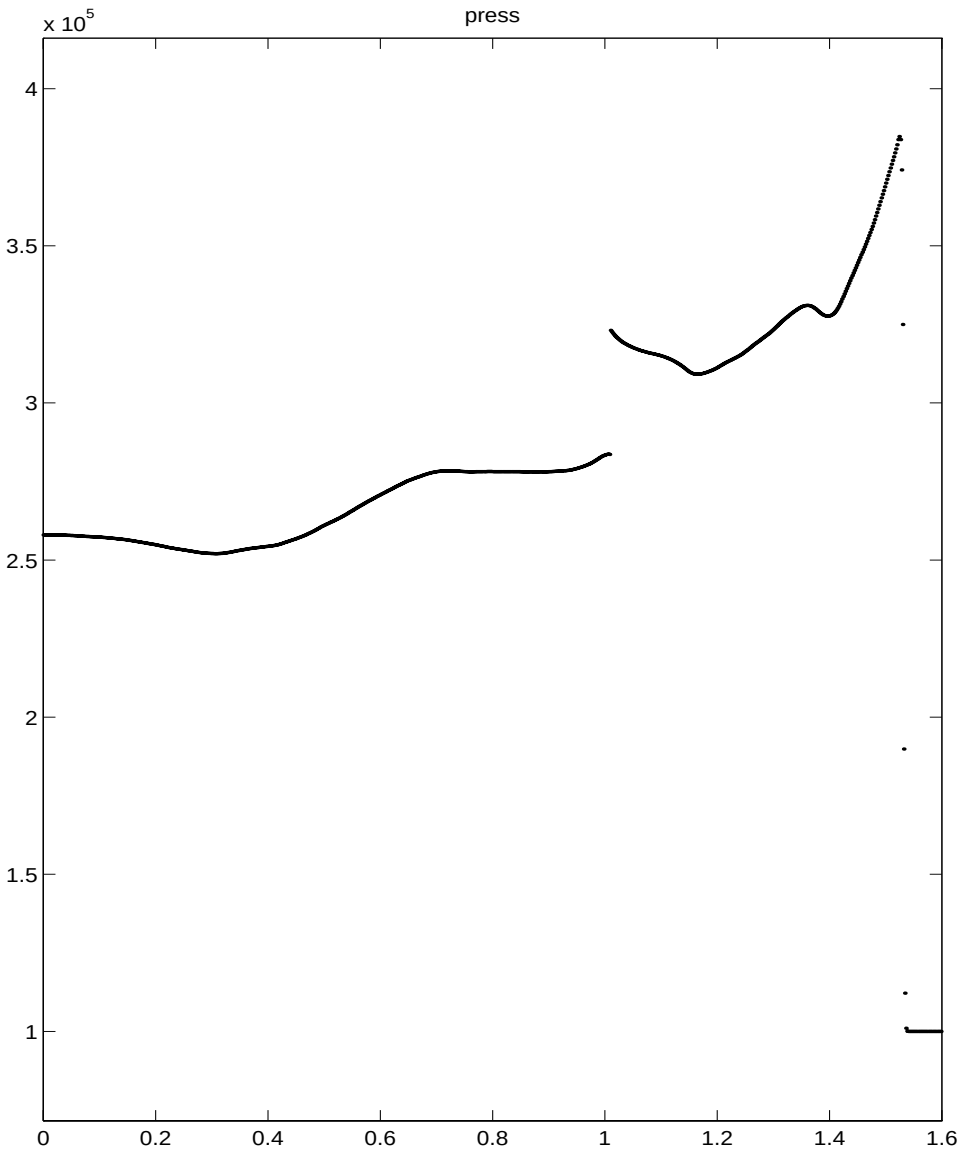

Figure 13: Deflagration Wave at $t = .0022s$

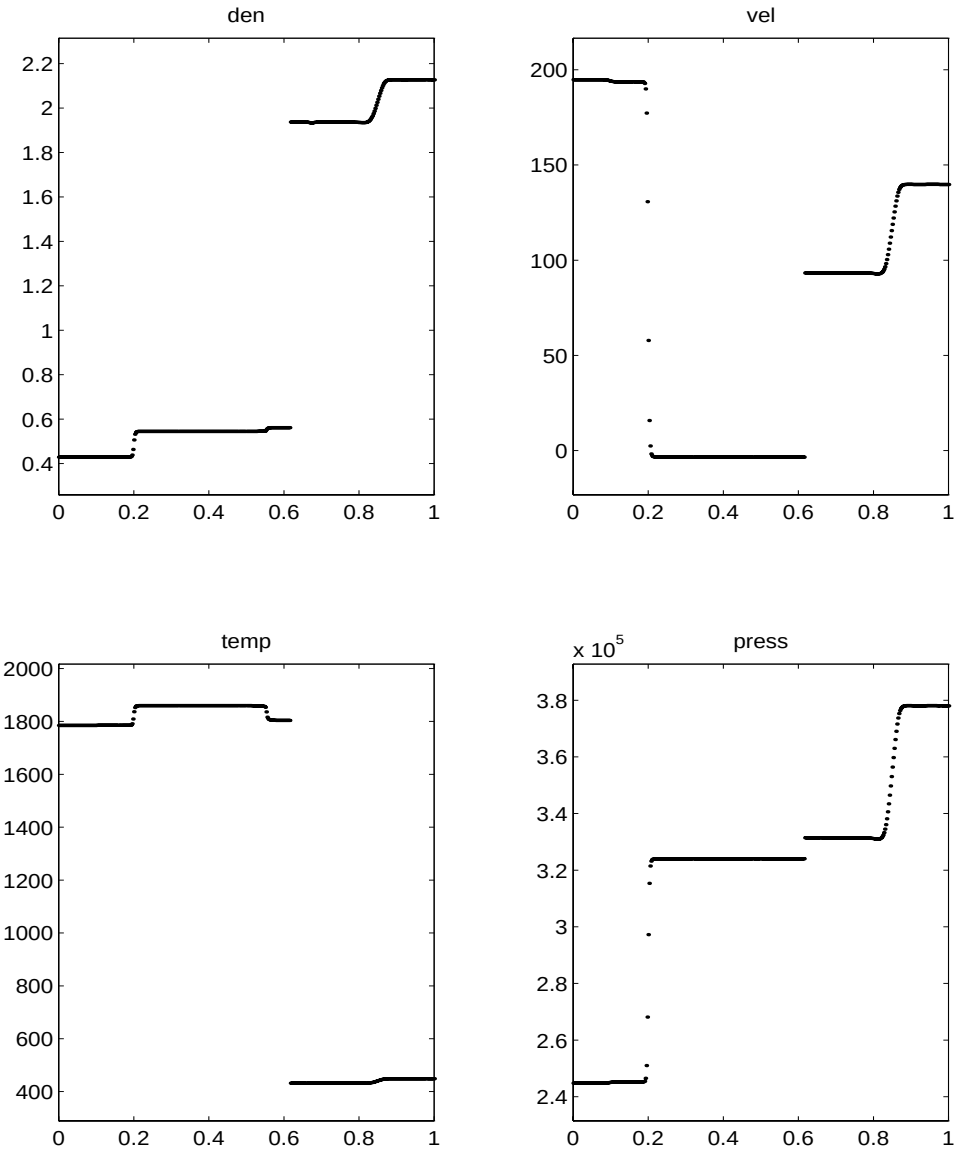

Figure 14: Deflagration interaction with a leftgoing shock

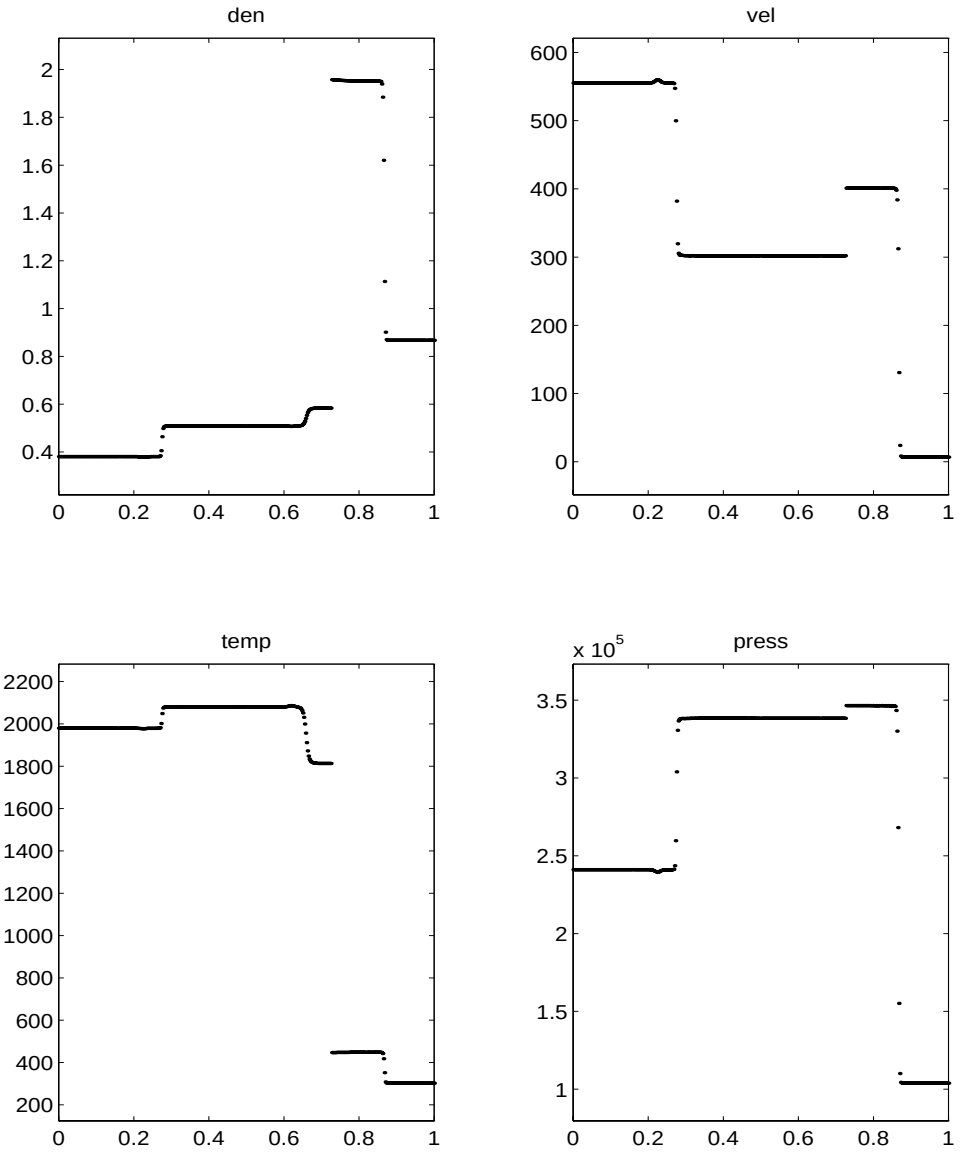

Figure 15: Deflagration interaction with a rightgoing shock

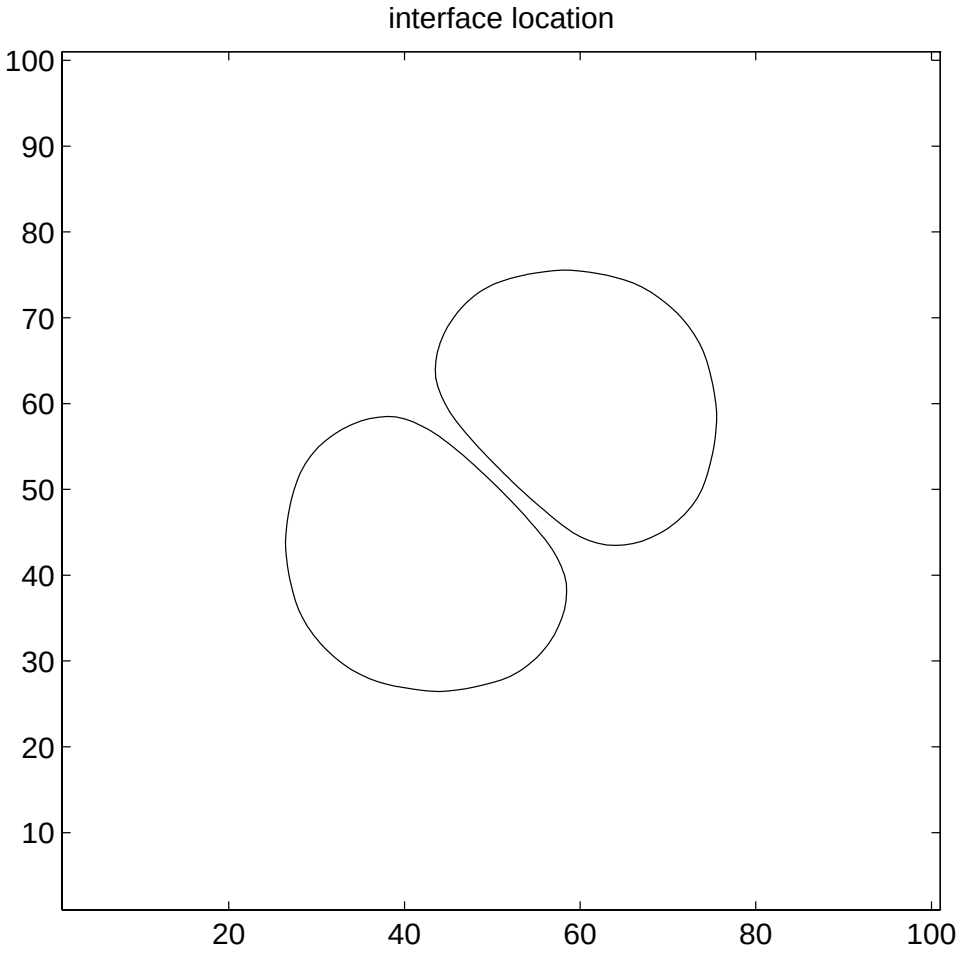

Figure 16: Before merging - .0008 seconds

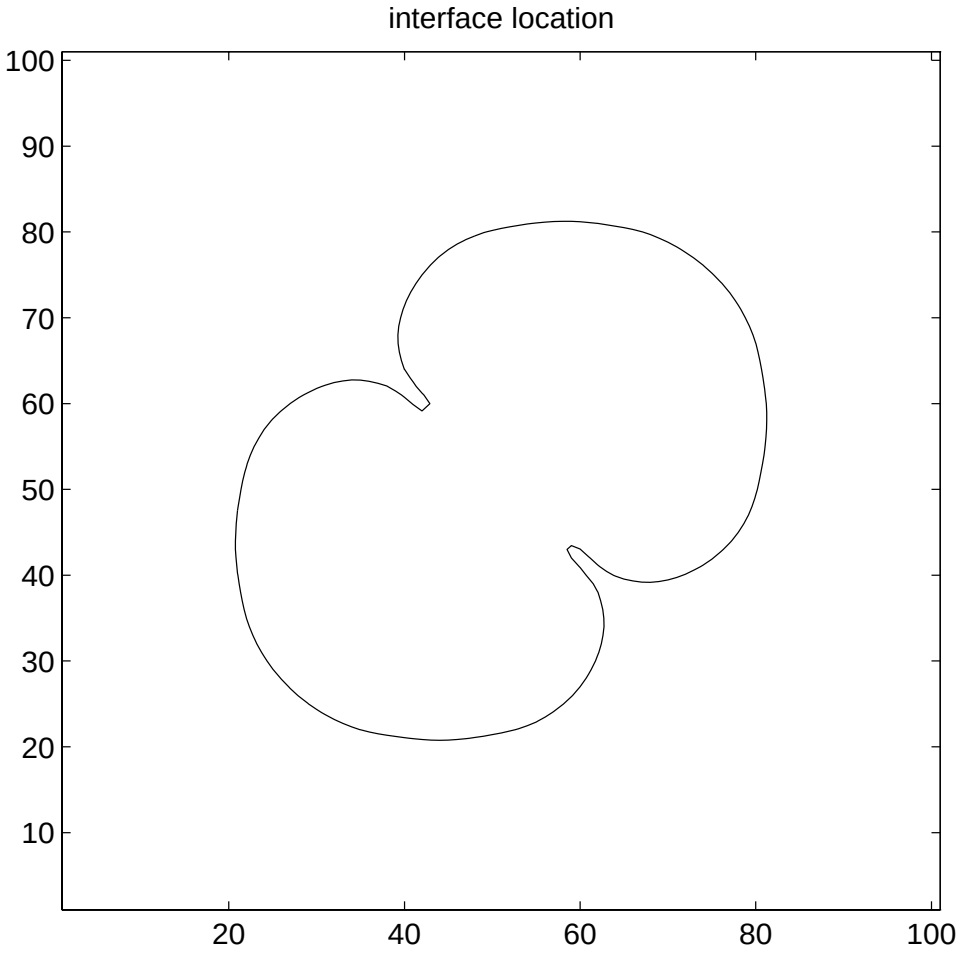

Figure 17: After merging - .001 seconds

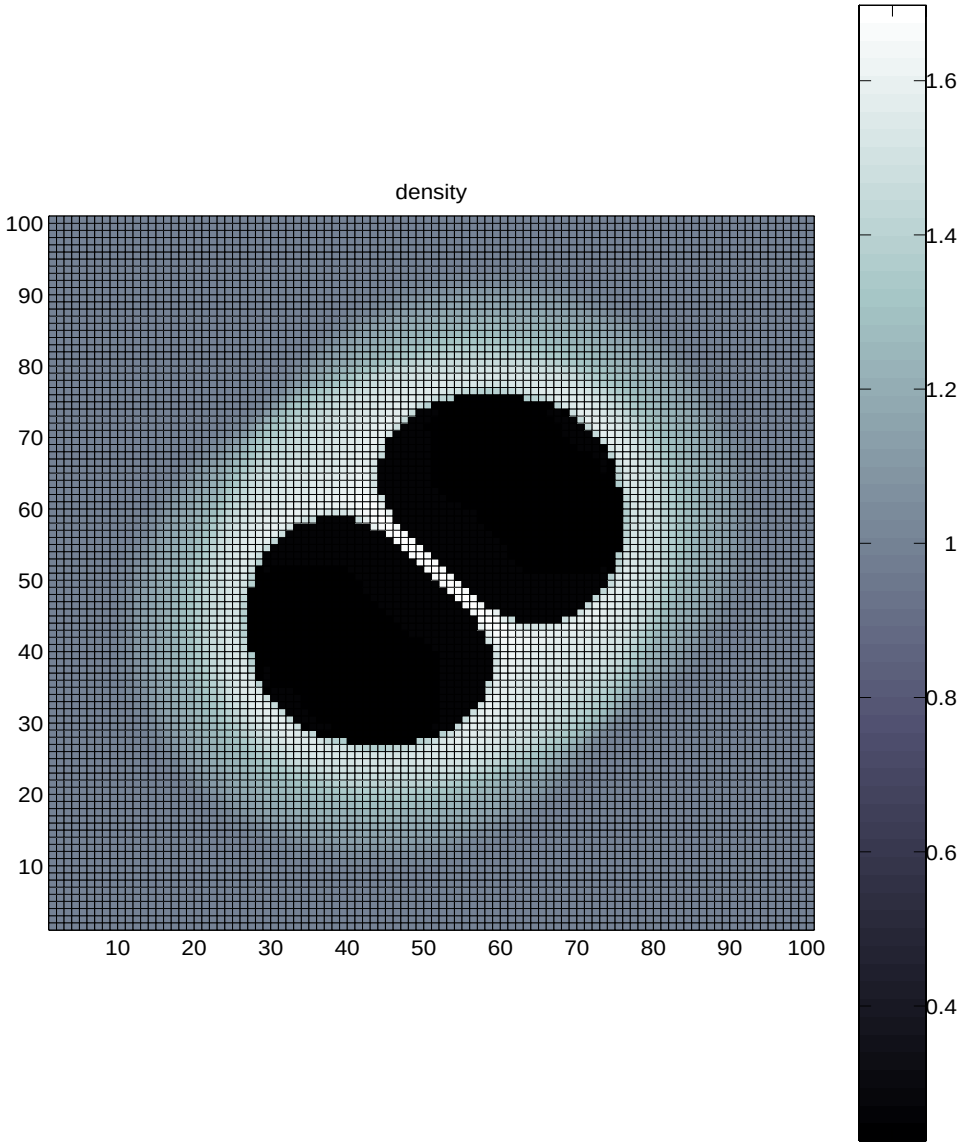

Figure 18: Before merging - .0008 seconds

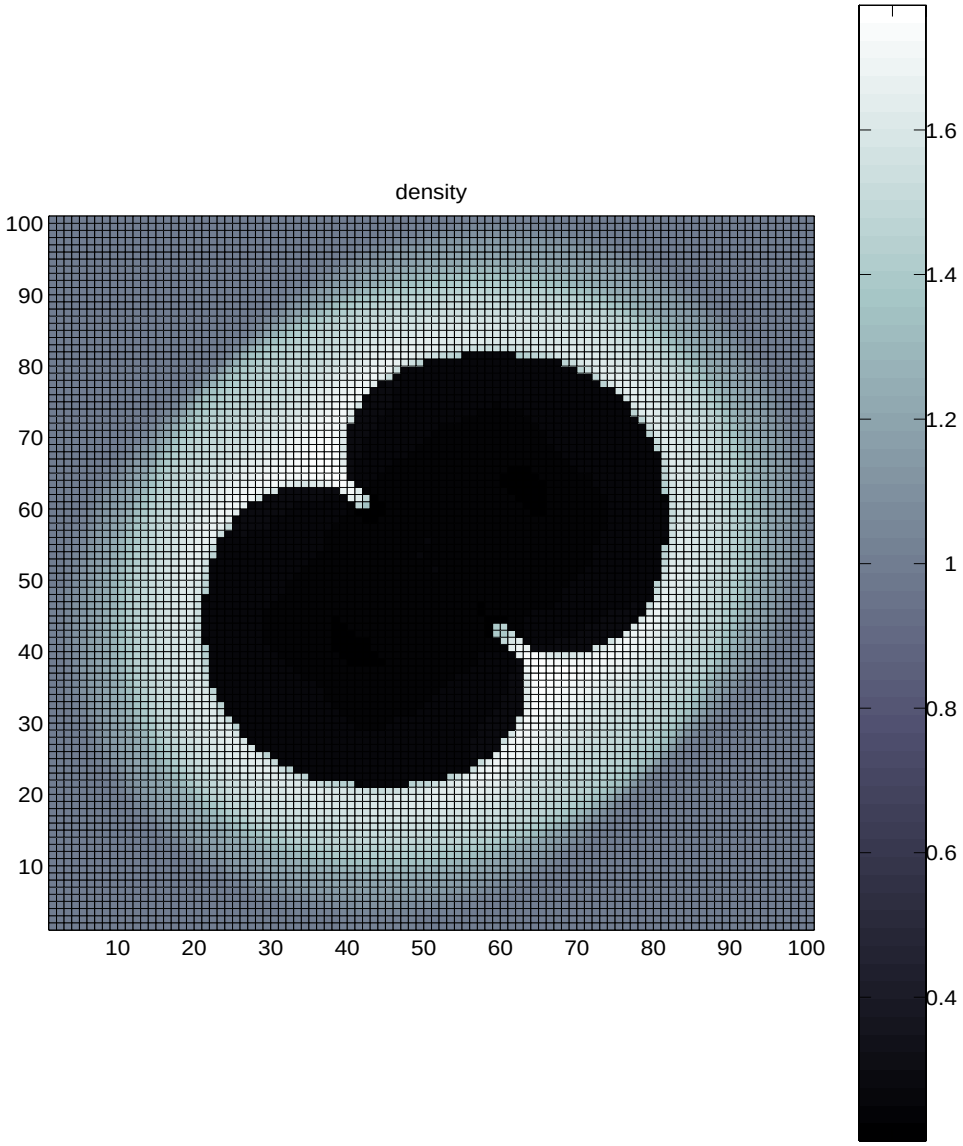

Figure 19: After merging - .001 seconds

References

[1] Aslam, T. *A Level Set Algorithm for Tracking Discontinuities in Hyperbolic Conservation Laws II: Systems of Equations*, (in preparation).

[2] Atkins, P., *Physical Chemistry*, 5th edition, Freeman, 1994.

[3] Cocchi, J.-P., Saurel, S., *A Riemann Problem Based Method for the Resolution of Compressible Multimaterial Flows*, Journal of Computational Physics, vol. 137, (1997) pp. 265-298.

[4] Davis, S., *An interface tracking method for hyperbolic systems of conservation laws*, Applied Numerical Mathematics, 10 (1992) 447-472.

[5] Fedkiw, R., Aslam, T., Merriman, B., and Osher, S., *A Non-Oscillatory Eulerian Approach to Interfaces in Multimaterial Flows (The Ghost Fluid Method)*, J. Computational Physics (submitted).

[6] Fedkiw, R., Marquina, A., and Merriman, B., *An Isobaric Fix for the Overheating Problem in Multimaterial Compressible Flows*, UCLA CAM Report 98-5, February 1998, J. Computational Physics (to appear).

[7] Fedkiw, R., Merriman, B., and Osher, S., *Efficient characteristic projection in upwind difference schemes for hyperbolic systems (The Complementary Projection Method)*, J. Computational Physics, vol. 141, 22-36 (1998).

[8] Fedkiw, R., Merriman, B., and Osher, S., *High accuracy numerical methods for thermally perfect gas flows with chemistry*, J. Computational Physics 132, 175-190 (1997).

[9] Fedkiw, R., Merriman, B., and Osher, S., *Simplified Upwind Discretization of Systems of Hyperbolic Conservation Laws Containing Advection Equations, with Applications to Compressible Flows of Multiphase, Chemically Reacting and Explosive Materials*, UCLA CAM Report 98-16, March 1998, J. Computational Physics (submitted).

[10] Fedkiw, R., Merriman, B., and Osher, S., *Numerical methods for a one-dimensional interface separating compressible and incompressible flows*,

Barriers and Challenges in Computational Fluid Dynamics, pp 155-194, edited by V, Venkatakrishnan, M. Salas, and S. Chakravarthy, Kluwer Academic Publishers (Norwell,MA), 1998.

[11] Hilditch, J., and Colella, P., *A Front Tracking Method for Compressible Flames in One Dimension*, SIAM J. Sci. Comput., vol. 16, no. 4, pp. 755-772, July 1995.

[12] Klein, R., "Personal Communication".

[13] Karni, S., *Multicomponent Flow Calculations by a Consistent Primitive Algorithm*, Journal of Computational Physics, v. 112, 31-43 (1994).

[14] Liu, X.-D. and Osher, S., *Convex ENO High Order Multi-Dimensional Schemes Without Field-by-Field Decomposition or Staggered Grids*, UCLA CAM report 97-26 (1997), Journal of Comput. Phys. (to appear).

[15] Markstein, G.H., *Nonsteady Flame Propagation*, Pergamon Press, Oxford (1964).

[16] Moser, V., Zhang, F., and Thibault, P., *Detonation front tracking via in-cell reconstruction*, Proc. 3rd Ann. Conf. of the CFD society of Canada (Bannf), 1995.

[17] Mulder, W., Osher, S., and Sethian, J.A., *Computing Interface Motion in Compressible Gas Dynamics*, J. Comput. Phys., v. 100, 209-228 (1992).

[18] Mulpuru, S.R. and Wilkin, G.B. *Finite Difference Calculations of Unsteady Premixed Flame-Flow Interactions*, AIAA Journal, v. 23, no. 1, January 1985.

[19] Osher, S. and Sethian, J.A., *Fronts Propagating with Curvature Dependent Speed: Algorithms Based on Hamilton-Jacobi Formulations*, Journal of Comput. Phys., vol. 79, n. 1, pp. 12-49, (1988).

[20] Sethian, J.A., *Curvature and the Evolution of Fronts*, Comm. Math. Phys., 101, 487, (1985).

[21] Shu, C.W. and Osher, S., *Efficient Implementation of Essentially Non-Oscillatory Shock Capturing Schemes II (two)*, Journal of Computational Physics; Volume 83, (1989), pp 32-78.

[22] Smiljanovski, V., and Klein, R., *Flame front tracking via in-cell reconstruction*, Proc. 5th Int. Conf. on Hyperbolic Problems, Theory, Numerics, and Applications, 1995.

[23] Smiljanovski, V., and Klein, R., *Simulation of gas dynamic flame instability and DDT using in-cell reconstruction*, Proc. 6th Int. Symp. on CFD (Lake Tahoe, NV), 1995.

[24] Smiljanovski, V., Moser, V., and Klein, R., *A capturing-tracking hybrid scheme for deflagration discontinuities*, Combustion Theory and Modeling, vol. 1, pp. 183-215, (1997).

[25] Sussman, M., Smereka, P. and Osher, S., *A level set approach for computing solutions to incompressible two-phase flow*, J. Comput. Phys., v. 114, (1994), pp. 146-154.

[26] Teng, Z.-H., Chorin, A., and Liu, T.-P., *Riemann Problems for Reacting Gas with Applications to Transition*, SIAM J. Appl. Math, vol. 42, no. 5, October 1982.

[27] Williams, F.A., *The Mathematics of Combustion*, (J.D. Buckmaster, ed.), SIAM, Philadelphia, PA, pp. 97-131 (1985).